

The abyssal giant sinkholes of the Blake Bahama Escarpment: evidence of focused deep-ocean carbonate dissolution

Thibault Cavailhes*, Hervé Gillet, Léa Guiastrennec-Faugas, Thierry Mulder, Vincent Hanquiez

Université de Bordeaux (UMR EPOC – OASU CNRS 5805) Allée Geoffroy Saint-Hilaire, CS 50023 33615 Pessac, France

ARTICLE INFO

Article history:

Received 31 July 2021

Received in revised form 18 November 2021

Accepted 23 November 2021

Available online 4 December 2021

Keywords:

Carbonates
Sinkholes
Escarpments
Tectonics

ABSTRACT

This study reports the discovery of abyssal giant depressions located at the toe of the Bahamian carbonate platform, along the Blake Bahama structurally-controlled Escarpment (BBE) that exhibits up to 4 km of submarine elevation above the San Salvador Abyssal Plain (SSAP). Analysis of seismic reflection and bathymetric data collected during the CARAMBAR 2 cruise revealed the presence of 29 submarine depressions; their water depths range from 4584 m to 4967 m whereas their negative reliefs are elliptical in shape, range in diameter from 255 m to 1819 m, and in depth from 30 m to 185 m. The depression alignment trends are parallel to the BBE as well as to structural lineaments of the area, exclusively between 2200 and 5000 m from its toe, and overlies a buried carbonate bench in which a high-amplitude seismic anomaly has been detected. The depression density interestingly increases where the recognized structural lineaments intersect the BBE. Based on their physical attributes (i.e. location, jagged morphologies, water depths), we interpret these depressions as collapse sinkholes rather than pockmarks or plunge pools. The aforementioned observations suggest an atypical relationship between the spatial occurrence of the giant abyssal sinkholes, the carbonate platform tectonic structures, the buried carbonate bench that underlies the hemipelagites in the SSAP and the geomorphology of the area. According to the wider literature that reports fluid seepages along submarine carbonate escarpments, we propose that the ground water entrance during low sea-level stands, the dissolution of evaporites by meteoric water, the platform-scale thermal convection and the seawater entrance at the platform edge most probably collectively act in concert to favor the circulation of brines and therefore the corrosion within the Bahamian carbonate platform. These mechanisms are particularly efficient along the structural heterogeneities (e.g. the Sunniland Fracture Zone, SFZ) which act as fluid conduits localizing the dissolution and control the physiography of the area by maintaining the location of the sedimentary pathways. The dense fluids would migrate along the faults towards the BBE free edge and are subsequently trapped into the buried carbonate bench that laterally disappears below the low-permeability deep-sea hemipelagites of the SSAP. In consequence, the trapped corrosive fluids dissolve the carbonates preferentially along the tectonic structures such as the SFZ. They are this way at the origin of the BBE curvature and generate collapse-structures in the overlying fine-grained deposits finally resulting in the formation of giant abyssal sinkholes. This structurally-directed process of dissolution seems efficient to provide a brines density head to move out down to >4.5 km of water depth and is believed to have played a major role in the BBE 5–6 km erosional retreat.

© 2021 Published by Elsevier B.V.

1. Introduction

Localizing, describing and understanding the zones of the upper crust where the fluids enter, flow, are stored and leak, are critical to discuss and quantify the geo-bio-chemical fluxes between the lithosphere, the hydrosphere and the atmosphere of the Earth (e.g. Dickens, 2003). Fluid flow and dynamics have been extensively studied at convergent

and divergent continental margins whereas transform margins that constitute 16% of the world continental margins (Mercier de Lépinay et al., 2016) have almost never been investigated in detail. Focusing on fluid circulation in carbonate margins allows scientists to interestingly trace and discuss the supply, the storage and the release of chemical elements implied in carbonate platform diagenetic reactions (Staudigel et al., 2021) as well as document their geomorphologic consequences, leading to surprising submarine karstic landscapes (e.g. Land and Paull, 2000).

Since the 1970s, our 4D-conception of the upper crust fluid circulation has been significantly improved by the description and the analysis of offshore fluid circulation and related fluid-escape features

* Corresponding author.

E-mail address: thibault.cavailhes@u-bordeaux.fr (T. Cavailhes).

distribution and geomorphologies (e.g. King and MacLean, 1970; Hornbach et al., 2007). Most of the marine scientific community attention has been focused on *pockmarks* whereas *offshore sinkholes* appear to have been poorly investigated or even misinterpreted. Understanding the differences between these two types of offshore structures appears necessary at this point. In terms of implications, these offshore fluid-related collapse/expulsion features have major impacts on seabed stability, implying potential hazards to offshore infrastructures as well as to coastal infrastructures by changing the failure rock mechanics that potentially leads to geomorphologic evolution, submarine escarpment destabilization and possibly to tsunamis (e.g. Orange et al., 2002 and herein references). Secondly, their distribution affines our knowledge of the fresh/saline water distribution, storage and flows in coastal and marine systems where the freshwater supply to cities remains problematic (Garven and Freeze, 1994; Post et al., 2013). Thirdly, subseafloor fluid-circulation markers and associated fluid-escape feature distribution patterns have also helped the oil and gas exploration geologists, which have used their presence to detect offshore seepages related to underlying petroleum systems since the 1930s (Abrams and Segall, 2001). Lastly, long-term seeping fluids through the seafloor have been identified as the primary control for chemosynthetic benthic ecosystems that currently localize a poorly understood submarine high biomass and productivity (e.g. pockmarks: Dando et al., 1991; Ondréas et al., 2005; sinkholes: Biddanda et al., 2006; Mitchell-Tapping et al., 1999).

1.1. Pockmarks

King and MacLean (1970, p. 3141) first defined as pockmarks the structures discovered off Nova Scotia as follows “*Pockmarks are cone-shaped depressions... possibly formed by ascending gas or subsurface water leakage from underlying ... sediments*”. These crater-like features or submarine depressions commonly occur in fine-grained sediments, have circular to ellipsoidal depression shapes and can reach up to 4000 m in diameter (e.g. Cole et al., 2000; Michaud et al., 2005). They have been observed in all ranges of water depth, from shallow-water environments (e.g. ~–15/40 m; Baltzer et al., 2014) to deep-sea water (~–3160 m; Marcon et al., 2014) and are considered as giant pockmarks in the case where their diameter is greater than 250 m (Foland et al., 1999; Pilcher and Argent, 2007). They have been recognized in different settings such as open oceanic environment (e.g. Michaud et al., 2005), lakes (e.g. Chapron et al., 2004), active margins (e.g. Salmi et al., 2011), passive margins (e.g. Ondréas et al., 2005), volcanic ridges (e.g. Michaud et al., 2005), clastic environments (e.g. Sultan et al., 2010), carbonate environments (e.g. Backshall et al., 1979; Betzler et al., 2011) and even proposed for explaining extraterrestrial surface circular morphologies (e.g. Mars: Komatsu et al., 2011). Rare outcropping paleo-pockmarks have been described in onshore studies such as the ones from Cantabria in Spain or the southeast basin of France (e.g. Agirrezabala et al., 2013; Gay et al., 2019).

The fluid sources related to pockmarks commonly originate from shallow subsurface sediments (e.g. Baltzer et al., 2014), dewatering and degassing of the water/gas-charged sediments (Agirrezabala et al., 2013), buried salt diapirs (e.g. Taylor et al., 2000; Gay et al., 2019), drowned carbonate banks (e.g. Betzler et al., 2011), buried unconformities (e.g. King and MacLean, 1970), buried sedimentary channels (Pilcher and Argent, 2007; Gay et al., 2003; Ondréas et al., 2005), buried Mass Transport Deposits (Bayon et al., 2009) and/or underlying petroleum systems (Pilcher and Argent, 2007). The nature of the involved-fluids can be of various origins such as biogenic gas (e.g. Cole et al., 2000; Marcon et al., 2014) and thermogenic gas, gas hydrate destabilization (Pilcher and Argent, 2007), hydrocarbon seeps and/or sand injectites (Cole et al., 2000), fresh water seepage (Chapron et al., 2004) as well as brines and sulfides (e.g. H₂S; Etiopie et al., 2006).

1.2. Submarine sinkholes

Karstic landscape geomorphologies also commonly exhibit sub-circular depressions called sinkholes or dolines (e.g. Sauro, 2003; Gutiérrez et al., 2008; Yechieli et al., 2015; Parise, 2019). Sinkholes are typical surface expressions of karst landscapes on Earth and potentially on extraterrestrial bodies (e.g. Titan's sinkholes; Cornet et al., 2015). These either onshore or offshore striking features originate from underlying subsurface dissolution cavities (dissolved origin) in either evaporites, carbonates or quartzites, leading to surface collapse (e.g. Gutiérrez et al., 2014; Sauro et al., 2019). A necessary condition for forming large sinkholes seems to be a large amount of fluid flow through the system, which allows and maintains the effective dissolution of the soluble host rock (Hiller et al., 2014). Submarine sinkholes and karstic landscapes are surprisingly absent from extensive reviews (e.g. Klimchouk, 2009; Gutiérrez et al., 2014; Parise, 2019). Submarine sinkholes mostly occur in carbonates and have been interpreted as: (i) subaerial dolines (meteoric water-related) that have been drowned during sea level rise (e.g. Backshall et al., 1979; Rosenberg, 2019), (ii) Dissolution derived crater-like features that originate from an underlying thermal convection of volcanic or basement-hydrothermal systems (e.g. Yubko and Lygina, 2015; ~–2300 m; Michaud et al., 2018); (iii) Submarine dolines related to the subsurface mixing of fresh and/or saline waters that dissolve limestones in coastal zones (e.g. ~–450 m, Land and Paull, 2000; ~–575 m, Land et al., 1995).

Inactive pockmarks and most of the submarine sinkholes are difficult to discriminate because none of them expels fluids at the time of data acquisition. In a few cases, several relatively hot water seeps have been observed in sinkholes (e.g. groundwater; Biddanda et al., 2006; saline waters; Mitchell-Tapping et al., 1999). However, in terms of formation mechanisms, it is generally admitted that pockmarks are preferentially physically excavated by focused fluid expulsion in comparison to sinkholes that originate from dissolution and physical collapse, this latter process leading to jagged morphologies (Hovland et al., 2002; Judd and Hovland, 2009). Detailed studies of pockmarks did not reveal any systematic ejecta rim around the depression despite the physical excavation (e.g. Pilcher and Argent, 2007); it seems that the venting of fluids preferentially removes the fine-grained sediments by suspending them into the water column (Webb, 2009). The fluid movements giving birth to pockmarks or sinkholes can be favored along structural surfaces or rocky basements (e.g. Shaw et al., 1997; Etiopie et al., 2006), through fractures in the sediments (e.g. Marcon et al., 2014) and through fault-zones of different scales (e.g. pockmarks: Sultan et al., 2010; Micallef et al., 2011; sinkholes: Mitchell-Tapping et al., 1999).

In this paper, (i) we aim to address the type (sinkholes or pockmarks), the distribution, the morphometry and the different mechanisms at the origin of the abyssal giant depressions alignment located at the toe of the Blake Bahama Escarpment (BEE; Fig. 1). In doing so, we use the bathymetric/seismic data in order to (ii) document and discuss the interactions between the km-scale structural features of the area, the carbonate platform-scale circulation, the circular submarine depressions and the current-day geomorphology. To our knowledge, pockmarks and sinkholes have never been described on modern sea floor below the Carbonate Compensation Depth (CCD; ~–4000 m), in abyssal carbonate contexts (>3000 m of water depth), at the toe of a structurally-controlled mega-carbonate escarpment such as the BBE (>4 km-high). In addition, we have most probably localized the geomorphologic depressions at the toe of the Bahamian platform where ‘brines’ would seep, as suggested in the Paull and Neumann's model (1987); the Fig. 2 of their publication).

2. Scientific context and geological setting

2.1. Tectonic setting and platform establishment

The Bahamas are located along a transform continental margin and are underlain by a stretched pre-Triassic continental crust (Mullins

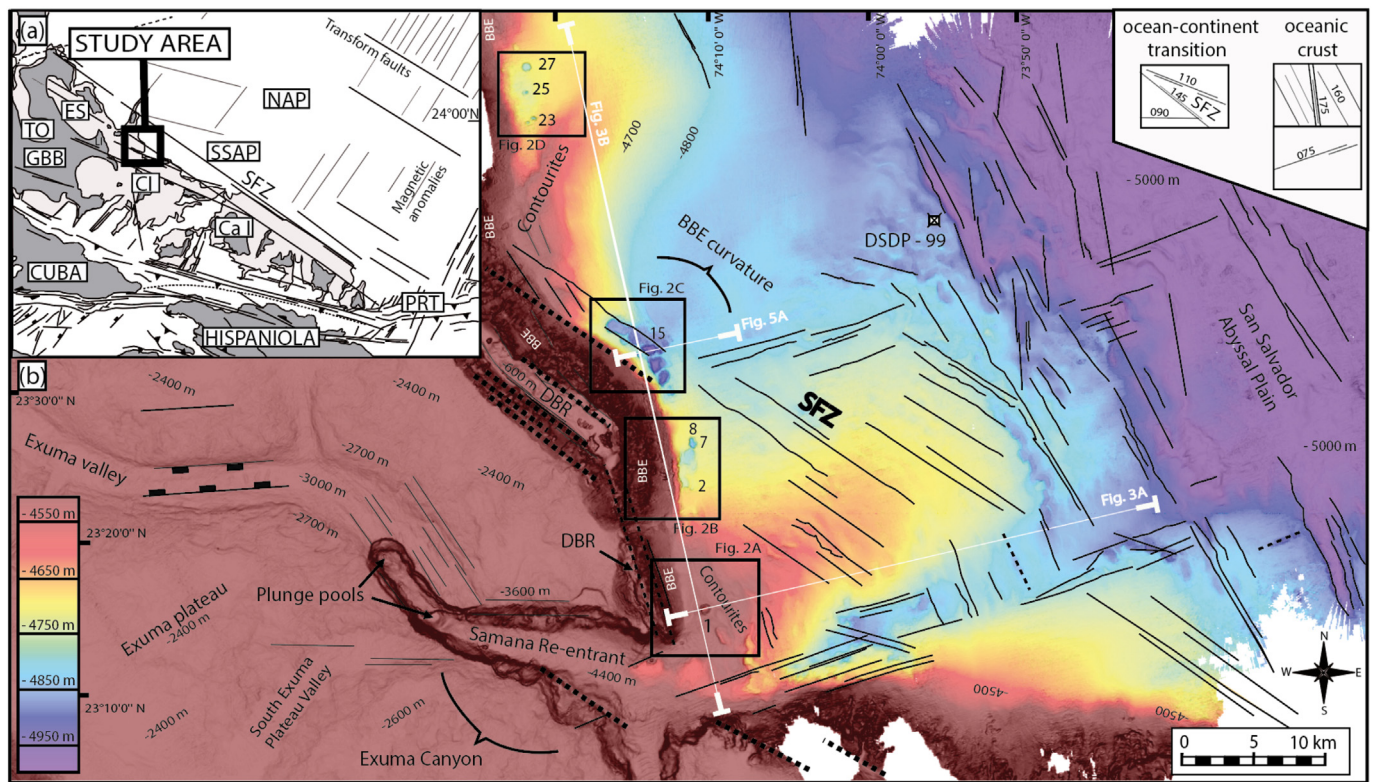


Fig. 1. (a) Structural Sketch of the Bahamas, Cuba and Hispaniola region. GGB: Great Bahama Bank, TO: Tongue of the Ocean, ES: Exuma Sound. SFZ: Sunniland Fracture Zone; NAP: North America Plate; CI: Crooked Islands; Ca: Caicos Islands. SSAP: San Salvador Abyssal Plain. PRT: Puerto Rico Trench. Dark grey is used for both platform water depth < 100 m, and the emerged areas. (b) Bathymetric data in the Exuma Canyon area where all the giant submarine depressions of this study have been recognized; -3600 m isobath is located within the BBE slope. The main structural lineaments (dashed straight lines) have been mapped according to their bathymetric, magnetic and gravimetric expressions. DBR: Drowned Barrier Reef. DSDP-99: Deep Sea Drilling Project, Site 99 (Hollister et al., 1972a).

and Lynts, 1977; Mercier de Lépinay et al., 2016) where a large carbonate platform developed in the Late Jurassic and Early Cretaceous in response to high carbonate production rates (Freeman-Lynde et al., 1981; Carlo, 1996). The clockwise rotation of the North American continental structural block caused a complex transensional ocean-continent transition where N-S striking normal basement faults (e.g. Blake Plateau) have coexisted with E-W striking pre-Jurassic basement Atlantic Ocean fracture zones (e.g. Blake Spur FZ, Great Abaco FZ; Sheridan, 1974). Since the early Cenozoic, active faulting occurred in response to the slight tectonic interactions between the southern Cuban orogeny and the Mesozoic-aged tectonic structures (Masferro et al., 2002; Kindler et al., 2011). Post-Oligocene reactivation of vertical basement faults have been reported by Mullins and Mark Van Buren (1981) in Walker's Cay (northern Bahamas), as well as a Neogene to present-day folding in the Santaren anticline (Masferro et al., 2002) and during the Quaternary tectonic tilting, using the Sunniland Fracture Zone along the Bahama escarpment (Kindler et al., 2011; Fig. 1a).

2.2. Carbonate platform circulation

Present-day carbonate platforms are commonly subject to dissolution, corrosion, dolomitization and dedolomitization by fresh and/or saline groundwater in the first kilometers deep (e.g. Sanford and Konikow, 1989; Hughes et al., 2007; Wierzbicki et al., 2006). This dissolution process can lead to relatively deep submarine sinkhole formation that are heterogeneously distributed, down to ~575 m in water depth (Land et al., 1995), i.e. deeper than the last glacial low stand of sea level (~120 m) and much shallower than the CCD (~4000 m). These geomorphologic markers of dissolution are important to characterize in order to address the architecture and the scale of fluid circulations in carbonate platforms.

2.2.1. Fluid circulation into the Bahamian platform

The Bahama platform offers within a same succession many reservoir rocks with a wide range of porosities (thick reefal and shallow water platform limestones and dolomites), organic matter-rich source rocks (restricted marine limestones) as well as the presence of vertical and lateral seals (fine-grained slope carbonate, pelagites and contourites, thick restricted marine anhydrites and halites), all needed for petroleum systems (Wallis, 1993). In addition, the Blake Bahama Escarpment (BBE) offers a 4 km-high and steepening with depth submarine topography that increases the vertical interacting section between groundwater and seawater, where the structural lineaments shape the submarine physiography. This provides an ideal case study to better constrain a structurally-controlled and dissolved carbonate system at the > km-scale. Indeed, water temperatures around faults into the Bahamian carbonate platform (depth: -3300 m to -3800 m) can be similar to water surface temperatures; these data demonstrate the direct and efficient hydrologic relations between surface and great depths (3500 m) (Wallis, 1993). Drilling and core data show that hydrodynamic alteration processes in carbonates near major fault surfaces create buried dissolution conduits and caves (e.g. 8 m high, porosity = 100%) at a depth of 4000 m in the Great Bahama Bank (Wallis, 1993). Solution collapse brecciation of dolomite sequences, in response to the dissolution of embedded anhydrites by corrosive fluids along faults, are suspected to cause those surprising reservoir properties within the platform.

Fluid circulation within the Bahamas carbonate platform has operated at different times, involving a wide range of fluid volumes, natures (freshwater, seawater and brines) and mechanisms; this has therefore needed efficient and long-term drivers of circulations (Melim and Masferro, 1997). The fluid circulation would be related to: (i) thermally driven circulation and density gradients between cold

saline oceanic waters and ground waters of the carbonate platform that are warmed by the geothermal heat flux (Kohout et al., 1977; Whitaker and Smart, 1990). (ii) Lateral flow due to an across-the-bank head difference (Whitaker and Smart, 1993; Whitaker et al., 1994) and the reflux of mesosaline brines along the platform (salinity of 38–45‰) that also drive circulation (Simms, 1984; Whitaker and Smart, 1990). (iii) The topographically-driven meteoric groundwater is probably a key factor for efficiently driving fluid-circulation into the carbonate platform, in particular during low sea-level stands (Wilson, 2005). The re-flooding of the banks at the last-deglaciation also strengthened the thermal convection (Dawans and Swart, 1988; Whitaker et al., 1994). (iv) Jointing optimizes the dissolution process by increasing surface areas exposed to corrosive waters (Freeman-Lynde and Ryan, 1985) and most probably enhances the existing circulation by supplying efficient, both porous and permeable km-scale structural-pathways for fluids. The structural heterogeneities of a platform are clearly the most efficient entities for fluid entrance, pathway, storage and seepage available spaces in carbonate rocks, allowing both episodic and persistent subsurface fluid-flows and overprinting an anisotropy of permeability in the faulted system i.e. the structural permeability (Sibson, 1996). At the cm-scale, pre-existing fractures and faults control the distribution, the orientation and the intensity of the carbonate dissolution by the circulating brines (defect-driven kinetic reactions); channelizing the shapes of dissolution targets of fractures and zones of structural weakness, preferentially along their strikes (Gouze et al., 2003; Garcia-Rios et al., 2015; Privalov et al., 2019). With the exception of onshore compressive settings (e.g. La Bruna et al., 2021; Pisani et al., 2021; Pontes et al., 2021), the structurally-controlled dissolution of carbonates, in particular in abyssal submarine settings, has not been described and is therefore poorly understood; this process remains to be documented at the km-scale, in particular for the Bahamian platform system.

2.3. Current-day physiography and escarpment basal erosion

The present-day steep morphology of the Blake Bahama Escarpment (BBE) has an erosional origin (~5–6 km of retreat, up to 4.2 km high), essentially developed during the Cretaceous (Freeman-Lynde and Ryan, 1985) and Tertiary times (Schlager et al., 1984). This probably still active erosional retreat overprinted a buried “bench-shaped” geomorphology exhibiting a relict ~5–6 km-wide flat carbonate surface currently buried by Miocene to Quaternary sediments lying in the San Salvador Abyssal plain (Schlager et al., 1984). Similarly to the Blake Escarpment (10–15 km of retreat), an Oligocene unconformity (A^u) is present at the top of the Cretaceous carbonates of the buried-bench and predates the Miocene massive sequences of turbidites and the Quaternary hemipelagites (Paull and Dillon, 1980). Contourites are present at the toe of the BBE at least since the Oligocene in response to abyssal currents activity (Bliefnick et al., 1983; Mulder et al., 2019).

More generally, the basal erosion of carbonate escarpments such as the BBE, the Blake escarpment or the Florida escarpment appears to be related to several non-exclusive mechanisms: (i) the circulating saline waters and brines that seep from the base of the escarpment dissolve the carbonates and therefore destabilize the overlying slopes (Wallis, 1993; Henderson et al., 1999; Paull and Neumann, 1987), such as described along at least 10% of the Florida carbonate Escarpment base (Paull et al., 1988; Chanton et al., 1991). These are made of 94% of seawater and 6% of dense brines (Chanton et al., 1991) and can reach temperatures up to 115 °C within the platform under Florida (Paull and Neumann, 1987). The combination of hydrogen sulfides (HS^-) and oxygenated seawater (from the platform edge) are suspected to favor acid (H^+) formation that corrodes the toes of a carbonate escarpment along open vertical fractures (Hill, 1990; D'Angeli et al., 2019). The slope of the BBE escarpment steepens with depth and inner platform carbonate facies at its base strongly suggests that collapse dismantlement operates in response to brine seeps. (ii) Locally, the tectonic activity related to movements along fracture zones implies rock jointing that increases

areas exposed to corrosive waters and slope destabilization (Freeman-Lynde and Ryan, 1985). (iii) The dissolution by oceanic corrosive waters would also imply escarpment undercutting, leading to overlying slope destabilization (Paull and Dillon, 1980), in particular for the anhydrite layers dissolved by ambient waters along the Florida escarpment (Paull et al., 1991). (iv) The removal of sediments and the lateral scarp retreat at the base of the slope by abyssal currents, suggested for the Blake escarpment and the BBE (Paull and Dillon, 1980; Schlager et al., 1984; Freeman-Lynde and Ryan, 1985; Land et al., 1999), have been excluded by Paull and Neumann (1987) for both Florida and Yucatan escarpments where abyssal currents are absent. In addition, (v) bioerosion has probably a very limited impact as argued in Freeman-Lynde and Ryan (1985). In contrast, the brine-related dissolution mechanism for explaining deep submarine karstic landscapes has been strongly challenged by Rosenberg (2019); the author proposes that all of the deep Florida and Yucatan sinkholes (water depth: –500 m to –2000 m) are related to a ~ one My-duration subaerial karstification event. This latter event would imply a ~ 2000 m relative sea-level fall related to the isolation of the Gulf of Mexico at the Paleocene that seems unrealistic for the Bahamas.

3. Methodology and database

Data set was collected during the Leg 2 of the CARAMBAR 2 cruise from December 2016 to January 2017 onboard the R/V l'Atalante (Mulder, 2016). The survey covered the southern part of Exuma Sound (ES), the Exuma Plateau (EP), the Blake Bahama Escarpment (BBE) and the adjacent San Salvador Abyssal Plain (SSAP), including 20,395 km² of multibeam bathymetry and backscatter and 2149 km of High Resolution (HR) seismic profiles. Bathymetry and backscatter data have been obtained using a Kongsberg EM122/EM710 multibeam echo sounder, and the high-resolution (HR) multichannel seismic system uses a 192 channels /1200 m long streamer (6.25 m group interval) and four 35/35 inc³ GI airguns. The signal dominant frequency is between 20 and 300 Hz. Streamer and source positioning were derived from vessel Differential Global Positioning System (DGPS) and compass birds. Processing of this seismic data was performed using SolidQC software developed by Ifremer. Basic processing flow included (i) Normal Move Out (NMO) correction, (ii) 24-fold stacking and (iii) constant velocity gradient migration. The obtained data are with vertical resolution approaching 2 m and usable acoustic imaging to approximately ca. 1 to 1.5 s two-way travel time. Sinkholes and structural lineaments have been mapped using their morphologic expressions such as depression, local changes in isobaths trends, as well as their seismic expression where 2D seismic data were available (Fig. 2).

4. Results

4.1. Submarine present day physiography

The studied area is located on an ocean-continent transition that has been shaped as a transform continental margin exhibiting a steep and sharp submarine morphology (Mullins et al., 1992; Mercier de Lépinay et al., 2016; Fig. 1a). The Sunniland Fracture Zone (SFZ) bounding the San Salvador Abyssal Plain is parallel to the oceanic transform faults and fracture zones identified on the sea floor of the North Atlantic Plate (NAP). This major tectonic corridor of tens of km wide trends perpendicular to the magnetic anomalies of the oceanic crust and clearly shapes the eastern side of the Bahamas submarine physiography (Fig. 1a). Only few morphologies and reliefs of the studied area are parallel to the N–S striking tensional basement faults recognized in Sheridan's works (1974) that control the Blake Plateau area shape.

Based on the analysis of bathymetric maps, the Drowned Barrier Reef (DBR), the Exuma Canyon (EC), the Samana Re-entrant (SR), the Exuma Valley (EV), the Exuma Plateau, the South Exuma Plateau Valley (SEPV), the Crooked Canyon (CC), the BBE, the plunge pools, and the

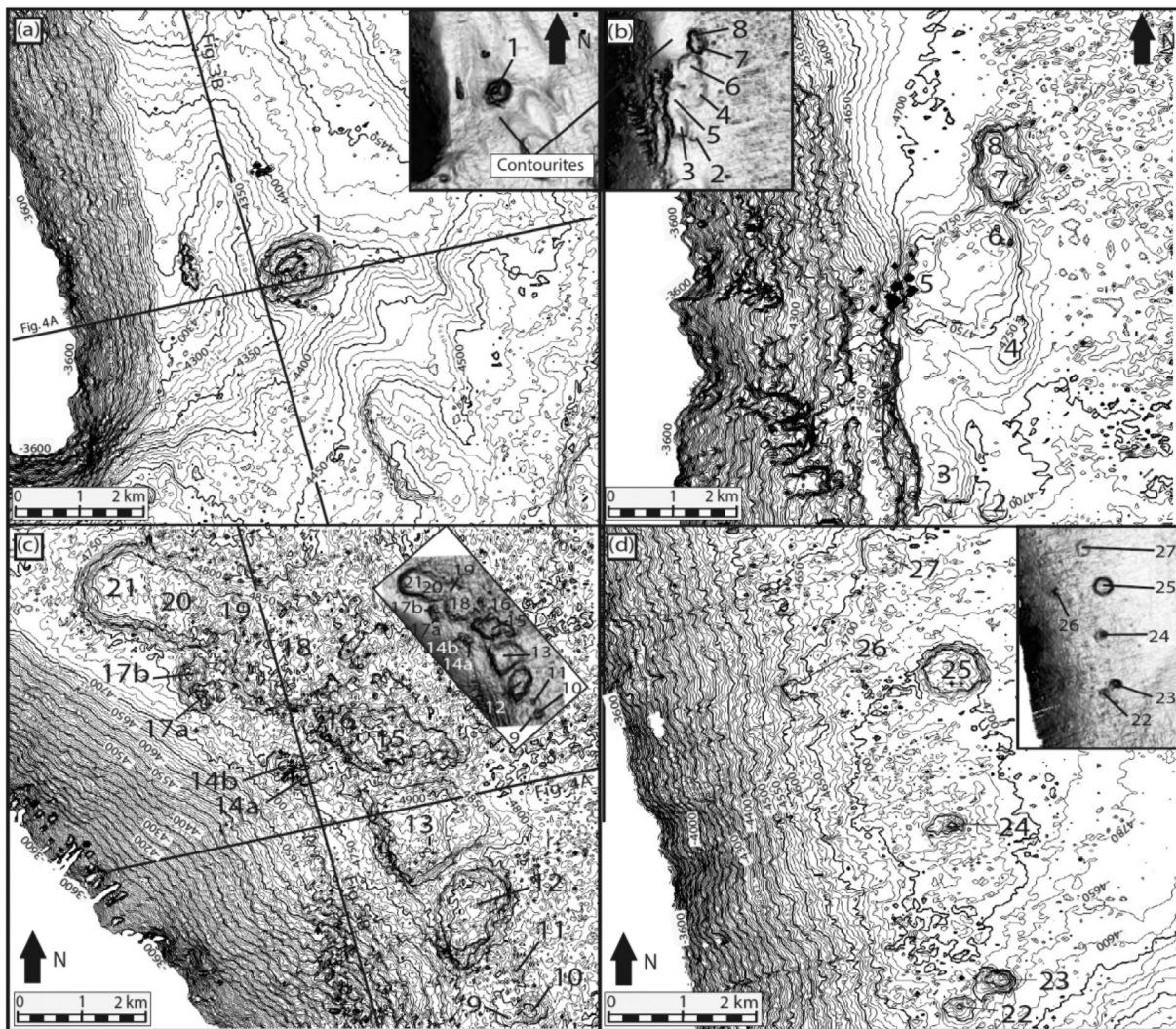


Fig. 2. (a) Details of the submarine depression 1 area where contourites are present. (b) Details of the depressions 2 to 8 area where inner chains and outer chains appear. (c) Details of depressions 9 to 21 area within the BBE curvature where inner and outer chains have been identified. (d) Details of the depressions 22 to 27 area. Slope maps are also provided for each bathymetric map.

contouritic deposits have been named similarly to the work of Mulder et al. (2019) (Fig. 1b). The generally N–S trending carbonate BBE can reach up to 4200 m of submarine elevation above the SSAP and is interestingly curved over a distance of ~18 km at $\sim 74^{\circ}10'W$; $23.32^{\circ}N$. The BBE curvature is observed in the area where the SFZ intersects the BBE. The SFZ appears to be made of different sets of tectonic features, striking N110, N145 and E–W (see inset in upper right corner of Fig. 1b). The 090E structural lineaments appear to control the shape of the southern part of the BBE, the northern edge of the Samana Re-entrant, the EV and the SEPV. The N110 and N145 trending lineaments (mean $\sim N130$ direction) control the submarine morphologies of the southern edge of the Exuma Canyon (Samana Re-entrant; SR), the transition between the EV and the SR, as well as the NW–SE trending BBE curvature (Fig. 1b). Regarding the oceanic crust structure in the SSAP, the lineaments are mostly N160 to N–S oriented and control the elongation of the distal lows where sediments are preferentially deposited (right part of Fig. 1b). In addition, the N–S basement-inherited BBE trend is very similar to the Crooked Canyon orientation. The contourites are present at the toe of the BBE (Mulder et al., 2019; e.g. Fig. 2a and b) with the exception of the BBE curvature area (Fig. 2c).

Summarizing these observations, the physiographic sketches of Fig. 1b reveal that ocean–continent transition inherited structural lineaments that control and shape the BBE trends and curvatures, the

submarine steep-walled giant canyon orientations (Mulder et al., 2019) as well as the abyssal topographies, clearly expressed by the structurally-controlled isobath contours. This structural architecture is consistent with the conceptual view of Sheridan (1974) arguing for the presence of structural blocks compartmentalizing the Atlantic continental margin by N–S tensional faults and major strike-slip features accommodating block rotation.

4.2. Regional distribution of submarine depressions

Twenty-nine abyssal submarine depressions have been mapped at the toe of the BBE, in the western part of the SSAP lying at ~ -4900 m of depth (Fig. 1b and 2); they occupy $\sim 20\%$ of the base of the carbonate escarpment, i.e. a total of 21.5 km/102 km long (Fig. 1b). The water depths of the depressions range from -4584 m to -4967 m, exclusively below the Carbonate Compensation Depth of the area (~ -4500 m; Heath and Mullins, 1984) (Fig. 2; Table 1). They are all located between 2 km and 5 km seaward of the toe of the BBE (isobath -4000 m). The mean depression diameters range from 255 m to 1819 m and form depressions ranging from 30 m to 185 m of depth without any clear preferential direction of elongation (refer to the Section 4.4 for details). The depressions of this study ($n = 29$) are so called ‘giant depressions’ considering that their diameters are wider than 250 m, following

Table 1
Quantification of sinkholes geomorphologic attributes.

Sinkhole number (from N to S)	Sinkhole water depth (m)	Sinkhole depth (m)	Distance (m) to the isobath "−4000 m"	Sinkhole length (m)	Length (°N) orientation	Sinkhole width (m)	Width (°N) orientation	Sinkhole mean diameter (m)
1	−4584	184	2965	1213	42	1115	132	1164
2	−4722	47	3428	548	20	357	110	452.5
3	−4739	39	2894	1045	159	697	249	871
4	−4772	47	3650	940	25	520	115	730
5	−4771	49	2474	1461	179	454	269	957.5
6	−4803	80	3087	1433	24	1008	114	1220.5
7	−4841	130	3563	756	176	753	266	754.5
8	−4824	109	3538	489	85	396	175	442.5
9	−4834	30	2943	255	154	183	244	219
10	−4871	47	3307	487	170	455	260	471
11	−4851	46	3336	288	151	223	241	255.5
12	−4933	96	3341	1733	22	1125	112	1429
13	−4950	176	3638	1712	144	1599	234	1655.5
14a	−4830	58	2709	447	151	312	241	379.5
14b	−4866	43	2842	388	145	288	235	338
15	−4966	151	4268	1330	93	1034	183	1182
16	−4967	138	3898	643	36	500	126	571.5
17a	−4835	87	2736	371	162	198	252	284.5
17b	−4857	97	2838	495	72	470	162	482.5
18	−4909	118	4114	1819	168	1765	258	1792
19	−4886	61	4011	710	93	680	183	695
20	−4891	133	3648	1584	172	1038	262	1311
21	−4897	151	3339	1552	22	1273	112	1412.5
22	−4757	67	3525	547	60	527	150	537
23	−4797	116	4171	748	90	385	180	566.5
24	−4812	118	3928	741	95	581	185	661
25	−4785	185	4648	1075	118	993	208	1034
26	−4681	81	2211	381	8	266	98	323.5
27	−4710	50	4079	762	152	630	242	696

the pockmark classification of Foland et al. (1999). Depressions are not randomly distributed in the studied area and show a high concentration nearby to the BBE curvature (Figs. 1b and 2c). Depression density increases where (i) the structural lineaments of the SFZ intersect the BBE and (ii) where contouritic deposits are absent. The depressions have been classified into two families: inner depressions ($n = 7$; $d_{\text{escarpment}} = 2\text{--}3$ km where 'd' is the shortest distance to the 4000 m isobath) and outer depressions ($n = 22$; $d_{\text{escarpment}} = 3\text{--}5$ km). In order to facilitate the description of the bathymetric map (Figs. 1 and 2), the depressions have been numbered from south to north (Fig. 2a to d); in the cases of 14a, 14b, 17a and 17b, each overlapping depression has the same number. This study distinguishes four areas of interest where a detailed analysis of abyssal depressions is considered (Fig. 2a, b, c and d).

Depression 1 is located in contouritic deposits and clearly appears isolated from the other depressions (7 km south of depression 2; Fig. 2a and b). It seems aligned with the E–W trending structural lineament bounding the northside of the Exuma Canyon and the southern depression described as a plunge pool in Mulder et al. (2019) (Fig. 1b). This is also, together with the depressions 23 to 27, one of the depressions of the study area that is collapsing contouritic deposits.

Depressions 2, 4, 6, 7 and 8 appear to be N–S aligned and located at ~3500 m from the BBE (Fig. 2b). In contrast, the depressions 3 and 5 are 1000 m to 2000 m closer to the BBE than 2, 4, 6, and 7, belonging to the inner depressions (Fig. 2b). The spacing between the depressions is between 0 m for the overlapping depressions (i.e. #7 and #8) and 1200 m (i.e. #2 and #4).

Depressions 9, 10, 11, 12, 13, 14a, 14b, 15, 16, 17a, 17b, 18, 19, 20 and 21 are located near the BBE curvature (~74°10'W; 23.32°N; (Fig. 2c)). More than half of the studied depressions (15/29) are therefore located where structural lineaments cross the BBE. Depressions 14a, 14b, 17a and 17b are called inner depressions because they are located at 2709 m and 2838 m from the BBE (Table 1). In contrast, the other depressions form a chain more distant to the BBE (around 4000 m; Fig. 2c). Contourites seem to be absent in this area (Fig. 1b).

Depressions 22, 23, 24, 25, 26 and 27 are located in the northern part of the studied area where a contouritic drift has been mapped (Fig. 1b). The depressions water depths range from −4710 m to −4812 m whereas the inner depression 26 is located at only 2211 m from the BBE, which contrasts with the others located at around 4000 m from the BBE (Fig. 2d; Table 1).

4.3. Seismic profile analysis

2D Seismic profiles and their interpretations are given in Figs. 3, 4 and 5. These figures exhibit two BBE-perpendicular-trending seismic lines (Figs. 3a, 5a) and one single BBE-parallel trending seismic line (Figs. 3b, 5b and c), which are all shown in Figs. 1, 2 and 3.

4.3.1. Sedimentary reflectors

The offshore seismic reflectors are believed to exhibit respectively from the subsurface to the surface, the top of the oceanic crust (basement), the top Kimmeridgian sedimentary package and the top of the Tithonian sedimentary package, consistent with the work of Schlager et al. (1984) (Fig. 3a and a). These interpreted sedimentary packages are westwards dipping and thickening, despite the fact their clear seismic expressions are blurring towards the BBE. The oceanic crust is around 0.3 s two-way travel time (TWT) deep in the eastern part of the profile whereas it is 1.2 s TWT deep in the western part of the profile. Due to this basement structural dip and the high sedimentary supply nearby the platform, the thickness of the sedimentary package reaches a maximum at the toe of the BBE (Fig. 3a). The Oligocene unconformity (A^u) has also been identified according to its high-amplitude seismic reflections, probably related to a strong lithologic contrast, as well as the recognized "downlaps" in the overlying Miocene deep-sea deposits (Fig. 3a; Paull and Dillon, 1980).

4.3.2. Buried bench

A 6 km wide buried carbonate bench exhibiting a typical blind facies is clearly identifiable in Figs. 3a and 5a and is similar in size and shape to

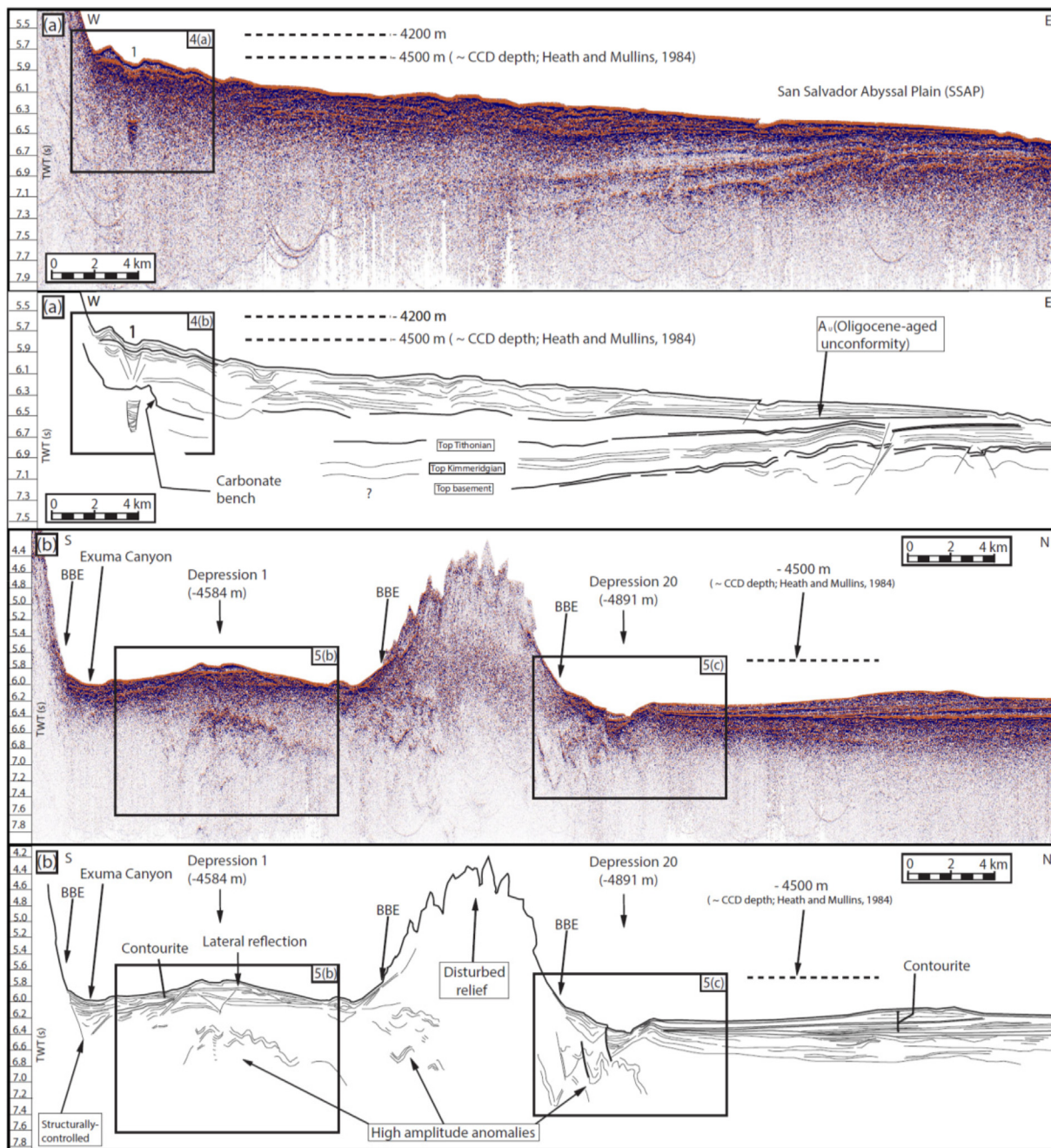


Fig. 3. 2D seismic lines Two-Way Travel Time (TWT) of the study area and associated interpretations: (a) N080 trending line respectively showing from the west (left) to the east (right) the BBE, the depression #1 and the San Salvador Abyssal Plain. The top basement, the top Kimmeridgian, the top Tithonian, the A¹ unconformity and the post Miocene deposits have been interpreted. (b) N170 trending line respectively showing respectively from the south (left) to the north (right), the Exuma Canyon, the depression #1, the BBE, the depression #2 and the layered northern contouritic deposits.

the one described at the toe of the BBE in Schlager et al. (1984). The top of this structure is located at around 6.5 s TWT and is overlain by contourites (Fig. 4a, b), except in the BBE curvature surrounding where it lies under a 0.2 to 0.3 s thick toe of slope hemipelagic cover (Fig. 5a, c, a and c). The seismic expression of the bench is also similar to the wider one (10–15 km) recognized at the toe of the BBE (Paull and Dillon, 1980). Subvertical seismic discontinuities within the bench suggest the presence of well-defined linear, antithetic and therefore “brittle-stylized” collapse faults (Fig. 4a, b). These faults have interestingly a “softer” shape in the overlying contouritic body, this latter being probably less lithified than the bench carbonates.

4.3.3. Bright spot

A seismic bright spot is defined as “a segment of a reflection on a near-vertical seismic reflection section which exhibits anomalously-high reflections amplitudes” (Makovsky and Klempner, 1999, p. 10795). The BBE - parallel seismic line crosses the BBE twice and exhibits diffuse high amplitude seismic anomalies (bright spot) between 6.4 s and 7.0 s TWT (Fig. 3b). The absolute depth of this feature is independent of the seafloor relief, the water depth or the vertical distance between the seafloor and this anomaly. This independency demonstrates that none of these parameters is a major controlling one, therefore suggesting that this feature probably originates from subsurface processes. The perpendicular trending seismic line exhibits a V-Shape structure (cone of

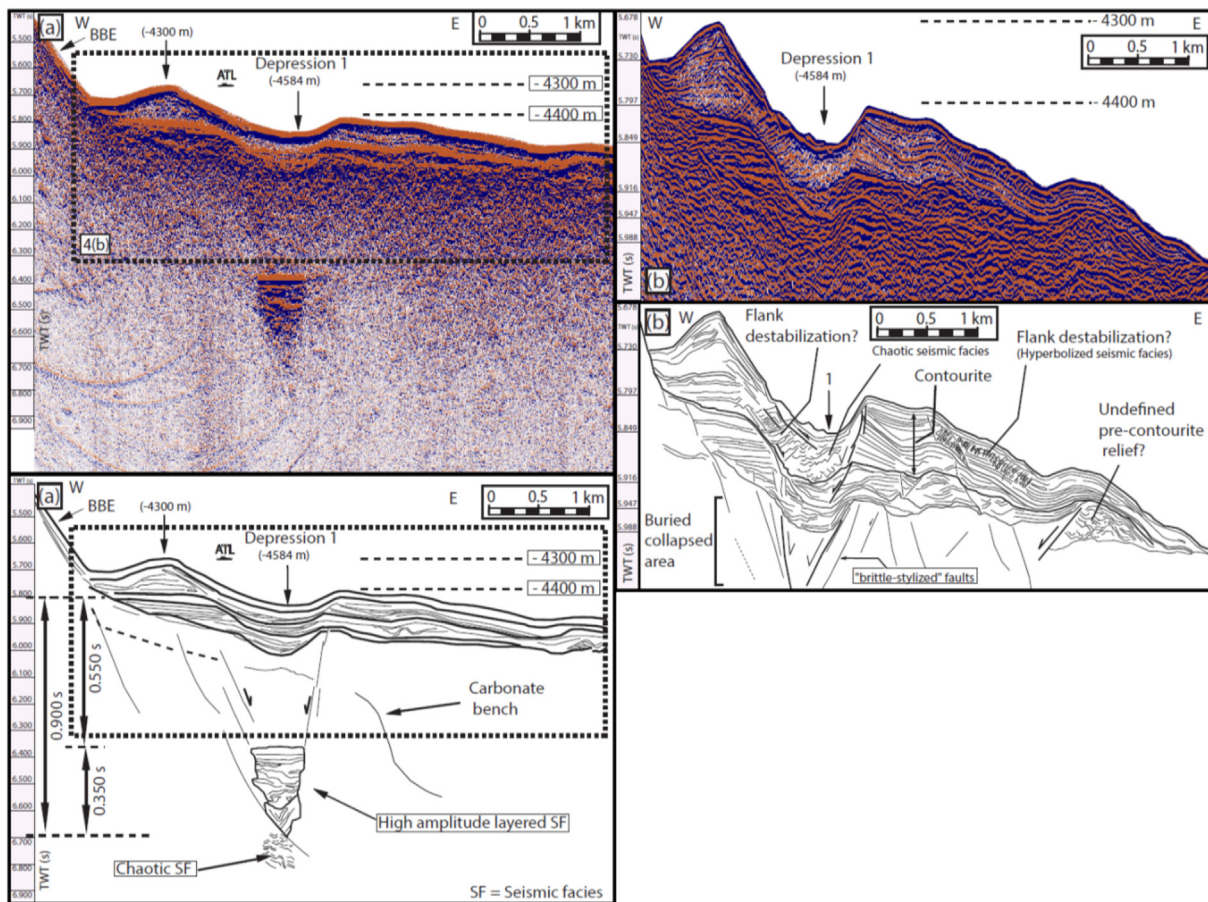


Fig. 4. (a) Details of Fig. 3(a) showing the depression #1 with its underlying seismic anomaly. (b) Details of the contouritic drift architecture overlying the depression #1 and exhibiting several stages of collapse by brittle faulting. The vertical exaggeration in (b) is around 2.5.

deformation) which is located right above the buried carbonate bench and terminates on the flank of the depression #1. The V-Shape structure is given by antithetic normal faults with sub seismic offsets that form a network apparently accommodating downwards collapse movement (Fig. 4b). The base of the V-shaped structure is located within the bench (Fig. 4b), between 0.6 s and 0.9 s underneath the seafloor depression. This bucket-shaped seismic bright spot shows a significant contrast between high-amplitude layered facies recognized in its upper part, the chaotic facies identified at its base and the low amplitude reflectors in the surrounding sedimentary rocks (Fig. 4a).

4.3.4. Contourites and depressions

The fine-grained deep-sea sediments represent the contouritic drift and are crosscut by depression #1 (Fig. 4b). This depression is bounded by at least four antithetic curved normal faults and shows a chaotic/disorganized facies in its center. The flanks of the depression are made of at least three phases of contourite deposition and show increasing sedimentary thicknesses at the vicinity of the depression (Fig. 4b). At least the upper package exhibits a hyperbolized seismic facies interpreted as a potential flank destabilization of the contourite drift (Fig. 4b).

We made a record of the acoustic response in the water column using the multibeam echosounder by positioning the boat just above depression #1 on the 23th of December 2016 (20h13–20h23 UT). There was no evidence for acoustic anomalies (upward motion of fluid plume) in the overlying water columns of this depression. The same measurement has been repeated on 28th of December (15h34–15h47 UT), within the water column above depression #15 with an identical result (Appendix 1).

4.4. Quantitative analysis

Water depths for the studied depressions are comprised between –4584 m and –4967 m (Fig. 6a). The deepest depressions are located within the BBE curvature where contourites are absent. The shallowest depression is the southern one (1) which is isolated (–4584 m) and perched on a contouritic drift. The inner depressions in the vicinity of the BBE curvature (i.e. 14a, 14b, 17a, 17b) are clearly shallower than the outer ones (9, 10, 11, 12, 13, 15, 16, 18, 19, 20, and 21). Consistently, the inner depression 26 is shallower than the 24, 25 and 27 outer ones.

All the giant depressions of this study are located between 2211 m (#26) and 4648 m (#25) away from isobath “–4000 m”, within the toe of BBE (Fig. 6b). The 7 inner depressions are located between 2211 m (#26) and 2894 m (#3) from the BBE whereas the outer depressions are located between 2943 m (#9) and 4648 m (#25) (mapping of inner and outer depressions is presented in Fig. 2). The greatest distances between the BBE and the outer depressions are systematically shorter than the BBE erosional retreat (5–6 km) proposed in Freeman-Lynde and Ryan (1985) and Schlager et al. (1984). This suggests that depressions appear to be always located immediately above the buried carbonate bench.

Depression mean diameters are related to depression shortest distances to the BBE according to the positive correlation of Fig. 6c. Two main trends can be identified on this graph, both including inner and outer depressions. For both relations, the closer to the BBE, the smaller is the depression.

Elongations have been measured for outer and inner depressions (Fig. 6d). Most of the depressions are slightly elongated

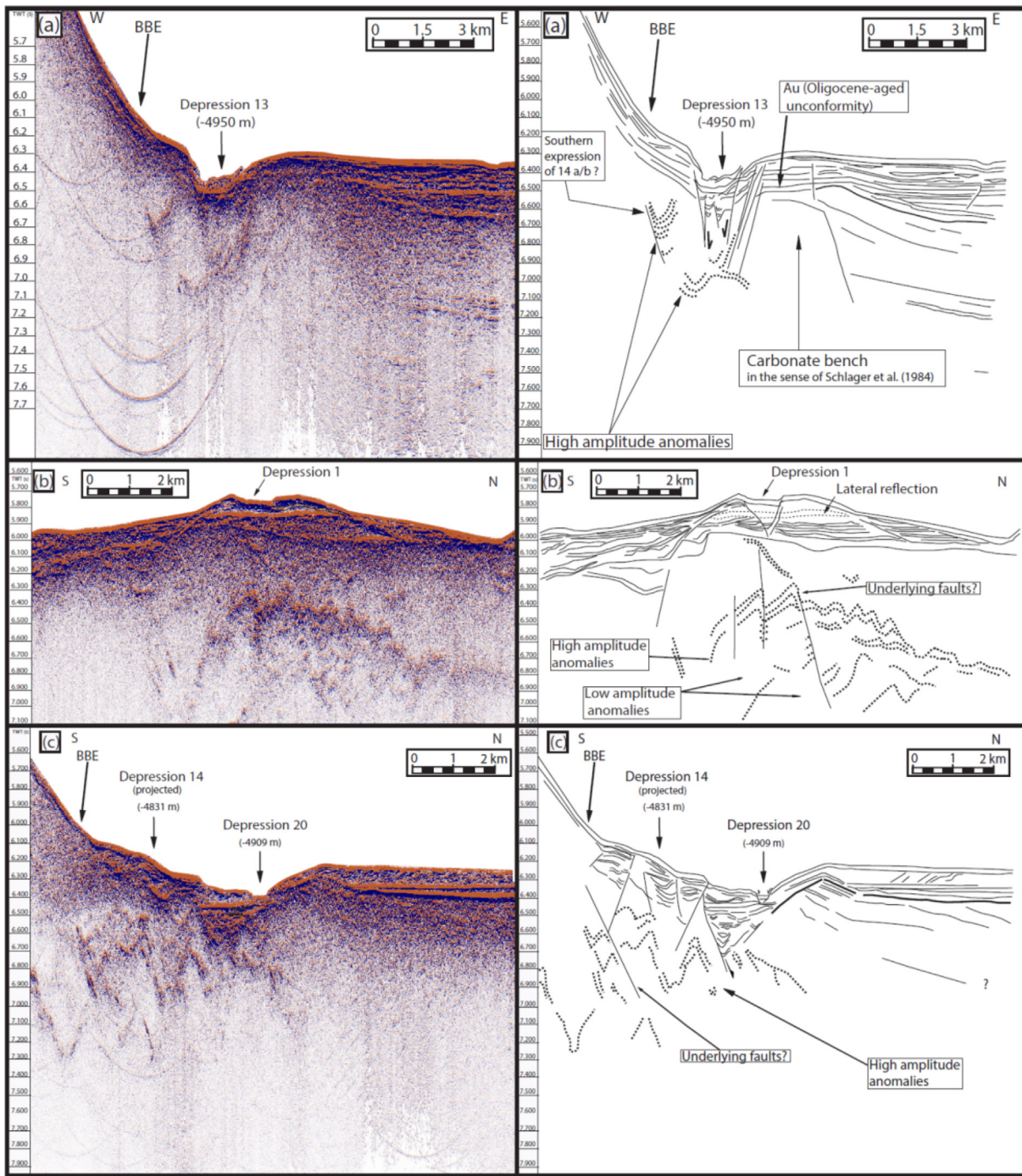


Fig. 5. (a) N080-trending 2D seismic line and its interpretation crossing the depression #13 in the BBE curvature area. (b) Details of the Fig. 3(b), 2D seismic line and its interpretation showing the depression #1 with its related underlying seismic anomaly. (c) Details of the Fig. 3(b). 2D seismic line and its interpretation showing the depression #20 near the BBE curvature area. The interpretation shows the normal faults probably related to the depression formation. The aforementioned seismic lines are also reported in Figs. 1 and 2.

with the exception of the inner depression #5, which probably originated from several underlying coalescent depressions. The related rose diagram highlights a N-S (from N020 to N160) and a N095 preferential direction of slight elongation (Fig. 6d; n_{max} elongation = 3). The inner depressions seem to be generally smaller than the outer ones.

The depression depths positively correlate with the depression mean diameters (Fig. 6e). The depression depths seem to be around 1/10 of the depression mean diameters. This scaling law is consistent with pockmark's scaling law from Pilcher and Argent (2007).

5. Interpretations and discussion

The studied abyssal depressions show strong morphologic similarities (size, depression depth and shape) with the submarine karstic structures described by Land and Paull (2000) along the carbonate continental slope of Florida (Fig. 6b). In addition, the morphologic sharpness of the studied depressions appears related to seafloor collapse (Fig. 5a and c). The depressions do not exhibit any evidence for fluid-assisted physical excavation that are commonly reported for pockmarks (Figs. 4b; Appendix 1). In consequence, despite being located in deeper

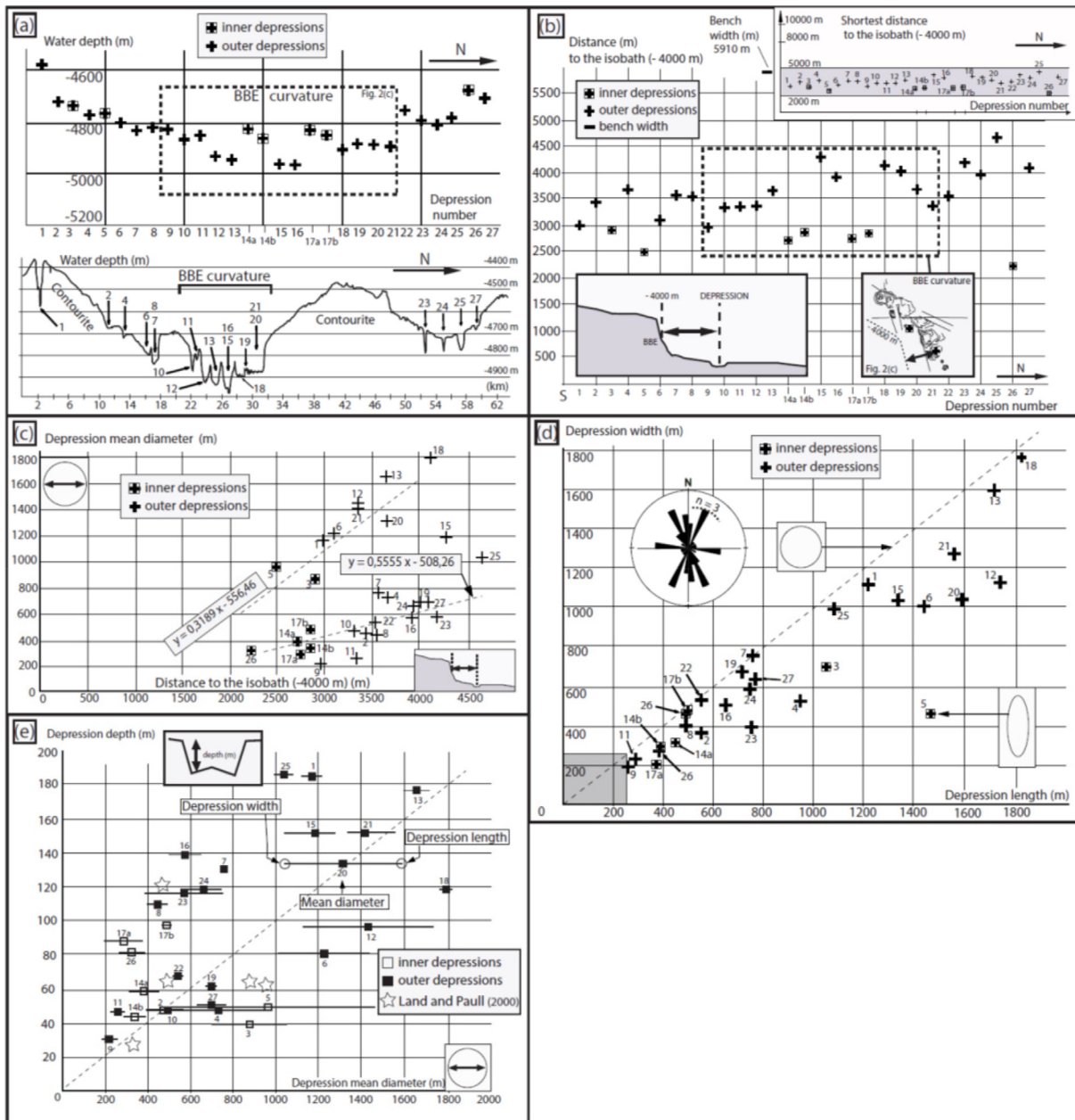


Fig. 6. Quantitative data: graphs showing (a) the water depth for the 29 depressions of this study and a related S–N bathymetric profile crossing the outer submarine depressions. (b) S–N depressions numbering as a function of the distance to the BBE, here expressed by the isobath (–4000 m). (c) Depression mean diameter as a function of the shortest distance to the BBE, dotted lines indicate two possible scenarios for data fitting. (d) Depression width as a function of depression length. Related rose diagram showing the slight elongation trend in the study area. (e) Depression depth as a function of the depression mean diameter. (For interpretation of the references to colour in this figure legend, the reader is referred to the web version of this article.)

water depths than the Florida depressions, we name these structures “abyssal giant sinkholes” (Figs. 7 and 8). The water depths (>4500 m) are important, so that we can confidently exclude a subaerial origin for the studied sinkholes and associated karstic landscapes. These newly discovered sinkholes are most probably related to an underlying hypogenic speleogenesis (Klimchouk, 2009) that could be related to either a brine-assisted dissolution of carbonates, as partly suggested by Paull and Neumann (1987), or to the dissolution of an hypothetical salt layer that has been not observed on seismic profiles (e.g. Warren, 2016; Fig. 3).

The physiographic sketch in Fig. 1 highlights that structural lineaments have most probably controlled and localized through times persistent and well-defined sedimentary pathways from the platform to the SSAP such as the Great Abaco Canyon (Mulder et al., 2018, 2019).

The studied abyssal sinkholes occupy 20% of the BBE toe and are preferentially localized where the inherited structural lineaments of the area cross the BBE (Fig. 1a). These observations demonstrate that a probable structurally-driven fluid circulation (leading to carbonate dissolution) along the lineaments and through the carbonate platform has likely played a key role during the erosional process leading to the retreat of the BBE. The deep-sea sinkholes growth have most likely destabilized the platform toe which is supported by the direct observations that this type of carbonate escarpments currently exhibits unstable submarine slopes steepening with depth, leading to one of the most pronounced topographic configurations on Earth (Paull and Neumann, 1987; Fig. 7). The BBE erosional retreat has therefore preferentially reused the inherited faults initially formed by the existing transform continental margin to reach its present shape (Fig. 7a).

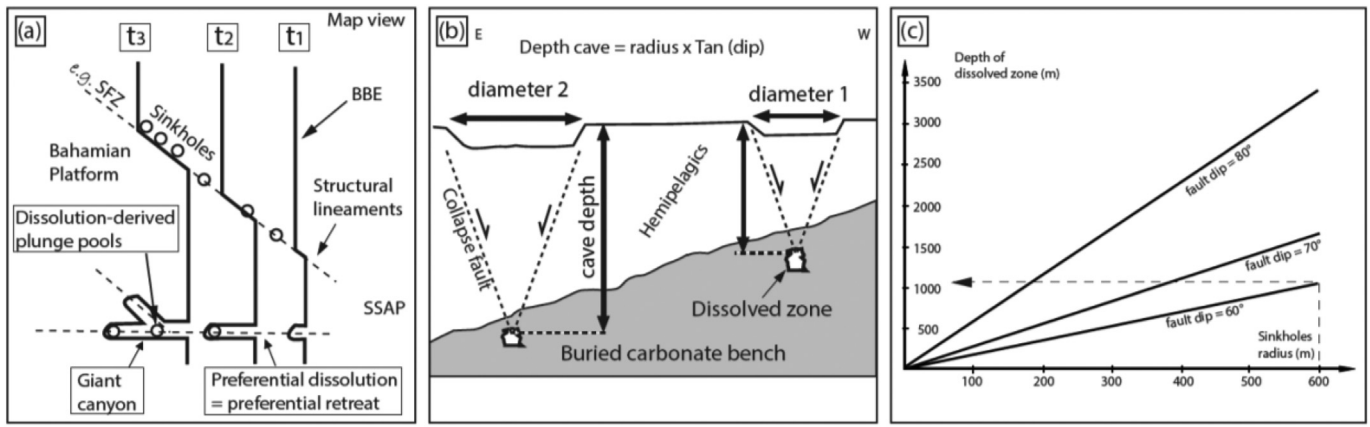


Fig. 7. (a) Conceptual sketch showing how the BBE erosional retreat likely exploits the structural lineaments related to the TOC transition in to reach its present-day geomorphological configuration. (b) Conceptual sketch showing the relationships between the depth of the dissolved rock volume (cave) and the radius of outer and inner sinkholes (c) Quantitative estimation of the cave depth in the case of sinkhole 1 (radius = 600 m).

Here, we (i) hierarchize the importance of the different controlling parameters explaining the sinkholes locations and we discuss (ii) the dissolving fluid origin and (iii) the platform-scale circulation. The structural, physical, chemical and time modalities leading to the current-day observed abyssal physiography are also discussed.

5.1. Controlling parameters for sinkhole's regional distribution

5.1.1. The distance to the BBE (first-order)

All of the discovered sinkholes are located at less than 4.7 km from the toe of the BBE, in this study expressed by the isobath - 4000 m (Fig. 6b). 6 km is the width of the buried carbonate bench described in Schlager et al. (1984) that is consistent with the amount of 5–6 km of

erosional retreat proposed in Freeman-Lynde and Ryan (1985). In this study, the 2D – seismic lines analysis corroborated that the aforementioned buried carbonate bench is present all over the area and in particular underneath the studied giant sinkholes (e.g. Fig. 5a). These results highlight the close relationship between (i) the toe of the escarpment, (ii) the sinkhole occurrence and (iii) the presence of the carbonate bench. Moreover, an N-S elongated sinkhole-underlying-seismic-anomaly (high amplitude) appears to be developed into the buried carbonate bench (e.g. Fig. 3b).

We here propose that a dissolution-related-cave-system at the origin of the overlying abyssal giant sinkholes would be currently expressed by the recognized underlying high-amplitude seismic anomalies and originates from the buried carbonate bench (Fig. 4a). This

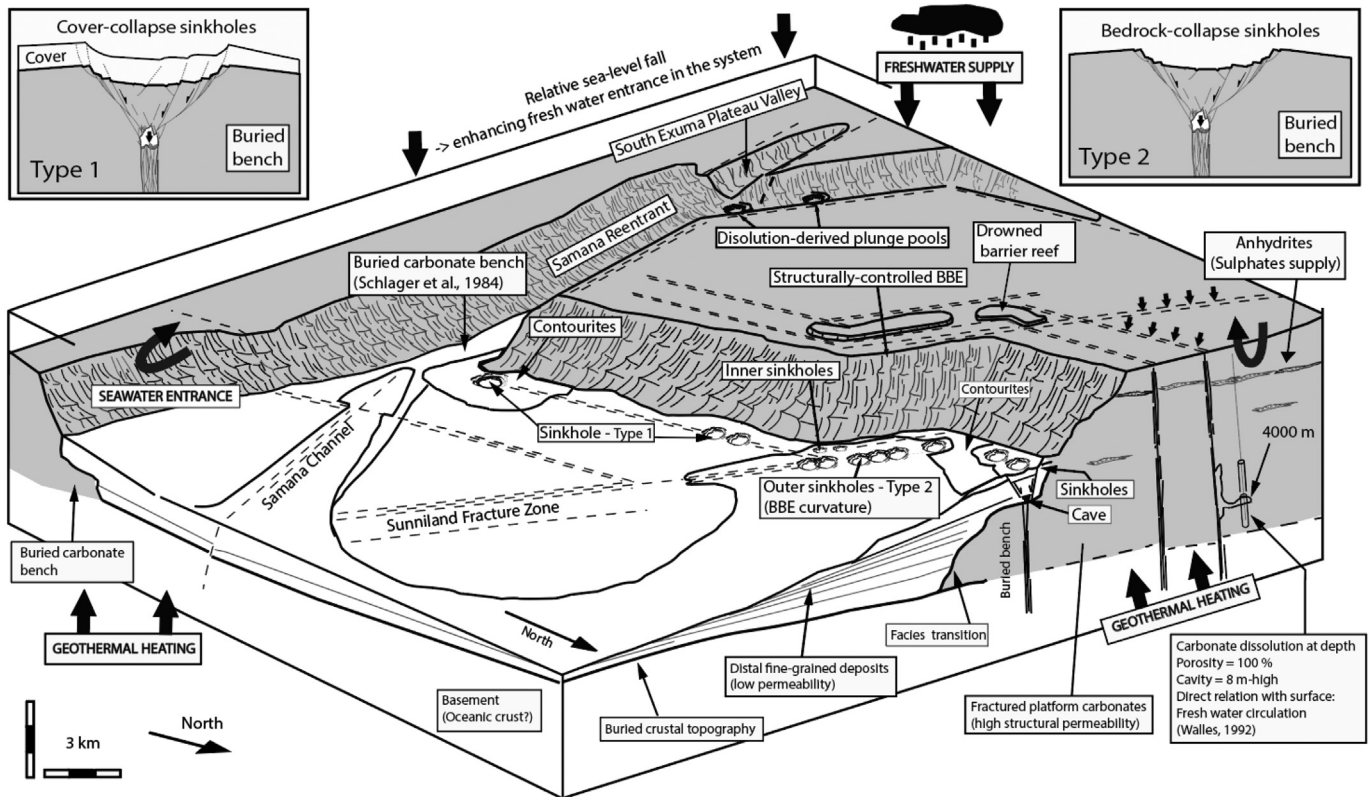


Fig. 8. 3D block diagram expressing the general understanding of the Blake Bahama Escarpment including our observations and the previous literature understanding (modified from Paul and Neumann, 1987). The brines are denser than sea water and would flow towards edge of platform. They would be trapped into the buried carbonate bench where the massive dissolution and related collapses both create the overlying observed sinkholes.

bright spot would represent either a collapse cave system related to dissolution such as extensively documented in Lu et al. (2017) for the Tarim basin deeply buried carbonates (~5500 m), or a non-understood seismic artifact (Fig. 4a). In addition to the carbonate dissolution, the bench may host evaporite layers that could also be easily dissolved and may therefore form large-scale caves (Warren, 2016). No evidence for acoustic anomalies in the overlying-sinkhole water columns (#1 and #15; Appendix 1) suggests that either no fluid was presently seeping from the sinkholes #1 and #15, or the fluid was not a gaseous gas or in adequate concentrations to be detected (Appendix 1).

5.1.2. The regional faults (second-order)

The highest density of sinkholes has been identified where the BBE is structurally controlled and shaped by the Sunniland Fracture Zone (SFZ; Kindler et al., 2011), leading to the BBE curvature (23°30'0"N in Fig. 1b, depressions #9 to #21 in Fig. 5a). This fact implies a causal connection between sinkhole location and structural lineaments in which the focused fluid migration is much more effective than non-focused flow through matrix porosities of the carbonate sedimentary column (Fig. 1; e.g. Pisani et al., 2021). The permeability of fracture corridors in carbonates, so called structural porosity, is commonly higher than the matrix permeability (e.g. Rotevatn and Bastesen, 2014). This is consistent with the preferential pathways used by the fluids to corrode and dissolve the buried bench (Fig. 7b). Strike-slip faults are more efficient than other faults to allow fluid flow along a vertical direction (Cavailhes et al., 2013) that is consistent with the SFZ inherited architecture which is considered as an inherited strike-slip tectonic structure (transform fault tip) related to the Atlantic Ocean opening. For instance, warm saline waters currently migrate upwards from the basement and through the SFZ in offshore Florida sinkholes (Mitchell-Tapping et al., 1999). In addition, Privalov et al. (2019) showed that, at the petrophysical sample scale (cm-scale), dissolution and corrosion in carbonates are both eased and preferentially localized along fractures, along which cavities more easily form and grow. At the karst scale, the fractures and faults are enlarged by the solutional widening (e.g. Kaufmann and Braun, 1999). In our case study, the structural heterogeneities are expressed at the large scale by the structural lineaments that control the dissolution distribution at the platform scale (sinkholes and dissolution-derived plunge pools).

The studied sinkholes show at least three morphometric similarities (i.e. diameter (~1 km), water depth (−4485 m; −4058 m) and presence along a structural lineament) with the *plunge pools* previously mapped in Mulder et al. (2018) (Fig. 1b). These latter only differ in terms of (i) location in the geological system i.e., located into the platform incising canyon and (ii) the depression depth (>300 m for *plunge pools*; <200 m for *sinkholes*).

5.1.3. Contourites, oceanic currents and buried sedimentary bodies (third-order)

Sinkholes can be present whether contouritic deposits are present (i.e. cover collapse sinkholes) or not (i.e. bedrock collapse sinkholes; see Gutiérrez et al. (2008) for the onshore terminology), therefore demonstrating that abyssal contouritic deposits did not favor or inhibit sea-floor collapses at the toe of the BBE. In addition, Fig. 4b shows that the sinkhole #1 growth and collapse both occur during the multiple phases of contourite deposition. This is consistent with an underlying carbonate dissolution by brines that would be independent of surface sedimentary processes (Fig. 7b). The studied sinkholes are elliptical in shape (Fig. 6) without any clear relation with the southwards stream bottom direction of the Deep Western Boundary Current (Lee et al., 1996). This means that based on our data, abyssal currents did not modify the studied sinkhole geometries. Post-sinkhole contourites may hide some underlying buried sinkholes, not identified neither on 2D seismic lines nor on the bathymetric map. Based on our 2D seismic analysis, no underlying buried sedimentary channels have been recognized

underneath the abyssal giant sinkholes of this study. This means that there is no additional buried sedimentary body (e.g. channels) at the origin of the storage of brines, with the exception of the carbonate bench.

5.2. Fluid origin and platform-scale circulation

5.2.1. Relation between the underlying cave depth and the sinkhole diameter

The inner sinkholes mean diameters are smaller than the outer sinkholes (Fig. 6c). This observation suggests a geometric relationship between the sinkhole diameters and their distances to the BBE. Indeed, for a similar buried cave size, the shallower the buried sinkhole cave, the smaller the diameter of the sinkhole should be because it (i.e. "the collapse structure") is bounded by normal faults (Fig. 7b; Gutiérrez et al., 2014). In consequence, we propose that the top of the buried bench, trapping the fluids, exhibits its own eastwards dipping slope, probably acquired during the Oligocene erosion phase (Paull and Dillon, 1980). Assuming a similar sinkhole collapse fault dips for all cases (either 60°, 70° or 80° in Fig. 7c) and using the Pythagoras theorem, we propose to quantitatively estimate the depth of the underlying dissolution-related cave location for the inner sinkholes. The base of the seismic anomaly (bright spot) where the sinkhole 1 roots is located at ~0.9 s below the seafloor i.e. 882 m–1035 m in depth, assuming V_p velocities in the range of 1.96–2.30 km/s (Hollister et al., 1972a, 1972b). These estimations seem consistent with a depth of ~1 km inferred from the 60° dipping normal faults and a sinkhole radius around 600 m (Anderson, 1951; Fig. 7c) commonly bounding collapse-sinkholes (Al-Halbouni et al., 2017).

5.2.2. Fluid circulation at the platform scale

At this stage, we do not have any direct evidence regarding the involved fluid nature, which would be responsible for such carbonate bench dissolution leading to sinkhole formation. However, based on the literature, the best candidate in terms of fluid chemistry would be the dense brine which is expected to seep at the toe of the BBE according to Paull and Neumann's work (1987). Our study suggests that these brines would be present down to 4.9 km of water depth according to the recognized geomorphological dissolution-markers (sinkholes). Whatever the fluids' chemistry, these inferences demonstrate that fluid circulation is active, significant and able to dissolve the carbonates (Hiller et al., 2014) through the entire thickness of the platform (>4.5 km of water depth). This fluid circulation is active and efficient in the area probably in response to the chemical/thermal fluids gradients as well as the high density of available structural pathways, in particular the Sunniland Fracture Zone (SFZ; Fig. 1). The purpose of this section is to qualitatively describe, synthesize and speculate on the architecture and the mechanisms of the fluid circulation in Bahamas-Florida Carbonate Platform (Fig. 8) such as proposed in Paull and Neumann (1987). Surface seawater and meteoric waters both infiltrate into faults and fracture corridors of the platform hosting carbonates (limestone, dolomite) and evaporites (anhydrites, halites) (Fig. 8). They may form a ~1 km-deep aquifer of fresh/sea water mixture in which part of the storage is matrix-located whereas water supplies are most probably structurally guided; indeed, relatively cold fresh water entrance has been for instance recognized at ~3600 m of depth into the Great Bahama Bank (Wallis, 1993; Fig. 8). Anhydrites such as the Cedar Key formation (Chanton et al., 1991) can be located at ~1 km depth into the platform (Hughes et al., 2007) and have a transitory barrier effect on the downwards fluid flow, efficiently compartmentalizing most of the fresh water circulation into the first kilometer. A fraction of this water would dissolve these anhydrites, therefore renewing its aggressiveness by incorporating acidic fluids (CO_2 , H_2S , SO_2), by increasing sulfate content in waters as well as water densities (Ford and Williams, 2007); this consequently promotes downward water movement within the platform. These brine-rich waters (SO_4^{2-}) would migrate horizontally eastwards to the free edge of the platform (~10.6 cm a^{-1} ;

Henderson et al., 1999), along the relatively high-permeability fault and fracture systems (Fig. 8; e.g. sinkholes and seeps along the SFZ in Mitchell-Tapping et al. (1999)). The brines would keep on flowing through the structural heterogeneities, towards the bench, due to their abnormal high density. They would be subsequently “trapped” into the bench where the host-rock platform carbonates facies laterally and vertically changes to low-permeability hemipelagic/contourite deposits. This phenomenon results in an identified area where the dissolution is probably focused (Corbella et al., 2004), in particular along the faults and fractures. An upward bounded solution feature forms at the top of the carbonate bench (Oligocene A^u-unconformity), inducing the formation of an overlying sinkhole as a surface expression of collapse in fine-grained sediments (Fig. 8; cover collapse sinkholes). Energy-rich fluids may seep from the sinkholes and fuel chemosynthetic food chains (Chanton et al., 1991; Mitchell-Tapping et al., 1999). Fluid-escape features that have been recognized by Paull and Neumann (1987) are decametric in scale whereas the mega-sinkholes of this study are 10 to 100 times larger. This is consistent with Mitchell-Tapping et al. (1999)'s observations as well as the model of Gay et al. (2019) showing sporadic decametric seeps within a giant submarine depression that act at different times as a function of available pathways in the sedimentary column and imply fluids lateral migration.

6. Conclusions

This work details and quantifies the distribution, the morphology and the vertical architecture of 29 newly discovered abyssal giant submarine depressions located at the toe of the BBE. Their origins and the mechanisms leading to a karstic landscape development are discussed together with the tectonic setting and the geomorphology of the area. The results and interpretations are summarized below:

- The studied submarine depressions are all giant (>250 m), abyssal (>3000 m of water depth) and atypically occur in carbonate settings below the CCD (>4500 m of water depth).
- The water depths (>4500 m) clearly exclude a subaerial origin for the studied sinkholes.

- Based on their bathymetric, their seismic profile expressions as well as their similarities with submarine Florida sinkholes, we propose that the studied submarine depressions are related to carbonate dissolution and can therefore be named collapse ‘sinkholes’. Sinkholes are preferentially located where the transform continental margin inherited structural lineaments controlling the Blake Bahama Escarpment morphology intersect the >4 km-high and steep submarine carbonate escarpment (BBE). The erosional retreat has preferentially reused the inherited faults, initially formed during the activity of the transform continental margin (such as the Sunniland Fracture zone).
- Sinkholes are all located along the BBE, at less than 5 km from its toe (−4000 m) and immediately above a buried carbonate bench shaped during the BBE erosional retreat.
- The dissolution of the carbonate buried bench, along faults and fractures, implied several stages of overlying collapse structures in the fine-grained deposits (contourites) and probable buried cave systems expressed by the recognized underlying seismic anomalies.
- According to Paull and Neumann's work (1987), the best candidate for explaining such carbonate dissolution at the toe of the BBE would be the brines. The dense brines most probably circulate along the structural heterogeneities of the entire Bahamian platform to finally occur at >4.5 km of water depth in this studied area.

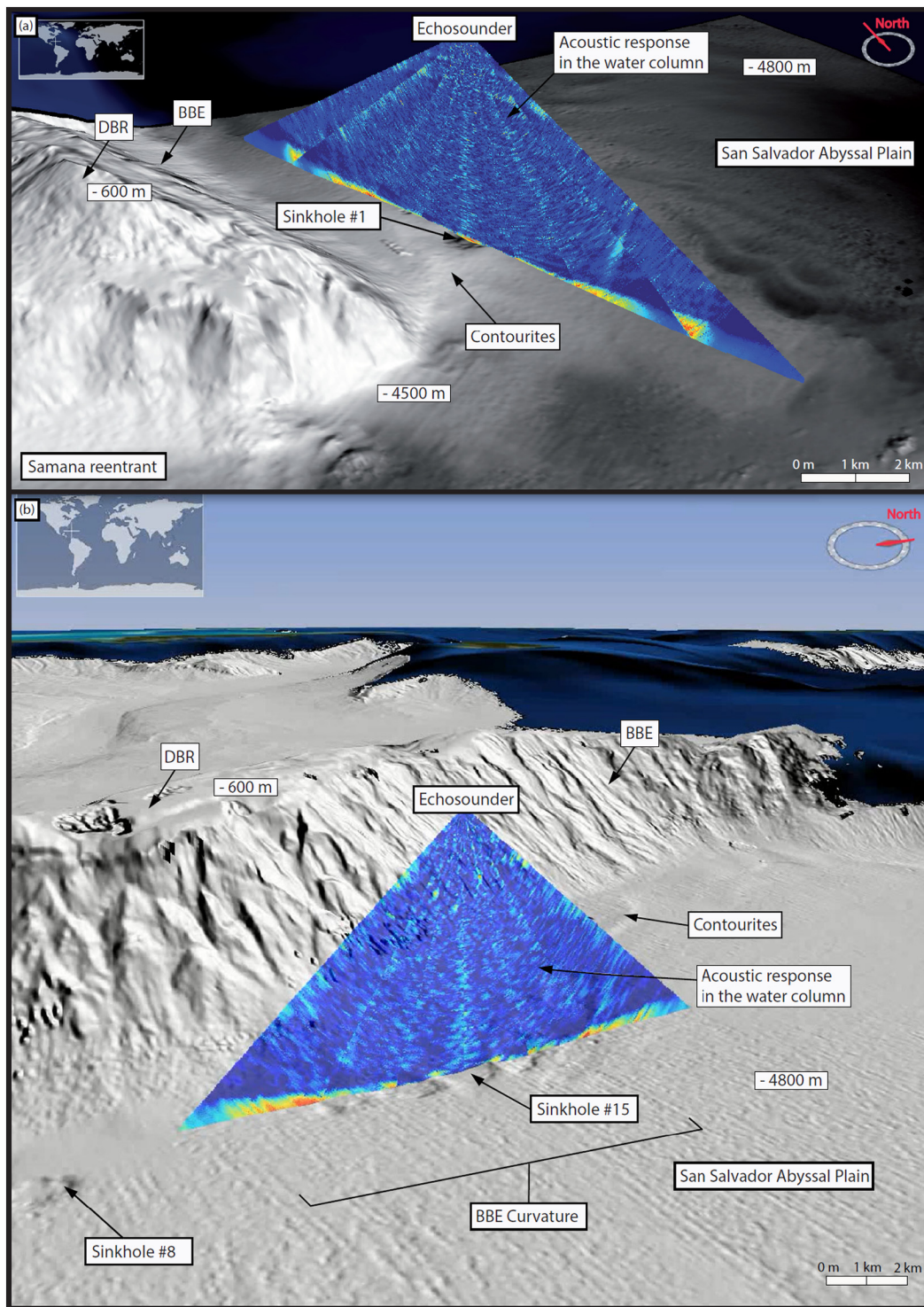
Declaration of competing interest

The authors (Thibault Cavailhes et al.) declare that they have no known competing financial interests or personal relationships that could have appeared to influence the work reported in this paper.

Acknowledgements

We thank Ifremer and Genavir (France) for cruise organization and technical support. We sincerely thank CharlesK. Paull, Jo De Waele, Francisco Gutiérrez and three anonymous reviewers for their constructive and accurate reviews on this manuscript. We acknowledge IHS for granting University of Bordeaux with academic Kingdom® software licences. We thank Yannick Thomas and Bruno Marsset for assistance in on board HR seismic reflection data processing with SolidQC.

Appendix A



Appendix 1. Acoustic responses in the water column above (a) the sinkhole #1 and (b) the sinkhole #15 that is located near the BBE curvature.

References

Abrams, M.A., Segall, M.P., 2001. Best practices for detecting, identifying and characterizing near-surface migration of hydrocarbons within marine sediments. Off-shore Technology Conference in Houston, Texas <https://doi.org/10.4043/13039-MS>.

Agirrezabala, L.M., Kiel, S., Blumenberg, M., Schäfer, N., Reitner, J., 2013. Outcrop analogues of pockmarks and associated methane-seep carbonates. A case study from Lower Cretaceous (Albian) of the Basque-Cantabrian Basin, western Pyrenees. *Palaeogeography Palaeoclimatology, Palaeoecology* 390, 94–115. <https://doi.org/10.1016/j.palaeo.2012.11.020>.

Al-Halbouni, D., Hologan, E.P., Saberi, L., Alrshdan, H., Sawarieh, A., Closson, D., Walter, T.R., Dahm, T., 2017. Sinkholes, subsidence and subsrosion on the eastern shore of

- the Dead Sea as revealed by a close-range photogrammetric survey. *Geomorphology* 285, 305–324.
- Anderson, E.M., 1951. *The Dynamics of Faulting and Dyke Formation With Applications to Britain*. Edinburgh, Oliver and Boyd.
- Backshall, D.G., Barnett, J., Davies, P.J., Duncan, D.C., Harvey, N., Hopley, D., Isdale, P.J., Jennings, J.N., Moss, R., 1979. Drowned dolines – the blue holes of the Pompey Reefs, Great Barrier Reef. *Journal of Australian Geology & Geophysics* 4, 99–109.
- Baltzer, A., Ehrhold, A., Rigolet, C., Souron, A., Cordier, C., Clouet, H., Dubois, S.F., 2014. Geophysical exploration of an active pockmark field in the Bay of Concarneau, southern Brittany, and implications for resident suspension feeders. *Geo-Mar. Lett.* 34, 215–230.
- Bayon, G., Loncke, L., Dupré, S., Caprais, J.C., Ducassou, E., Duperron, S., Etoubleau, J., Foucher, J.P., Fouquet, Y., Gontharet, S., Henderson, G.M., Huguen, C., Klauke, I., Mascle, J., Migeon, S., Olu-Le Roy, K., Ondréas, H., Pierre, C., Sibuet, M., Stadnitskaia, A., Woodside, J., 2009. Multi-disciplinary investigation of fluid seepage on an unstable margin: the case of the Central Nile deep sea fan. *Mar. Geol.* 261, 92–104.
- Betzler, C., Lindhorst, S., Hubscher, C., Ludmann, T., Furstenau, J., Reijmer, J., 2011. Giant pockmarks in a carbonate platform (Maldives, Indian Ocean). *Mar. Geol.* 289, 1–16. <https://doi.org/10.1016/j.margeo.2011.09.004>.
- Biddanda, B.A., Coleman, D.F., Johengen, T.H., Ruberg, S.A., Meadows, G.A., Van Sumeren, H.W., Rediske, R.R., Kendall, S.T., 2006. Exploration of a Submerged Sinkhole Ecosystem in Lake Huron. *Ecosystems* 9, 828–842. <https://doi.org/10.1007/s10021-005-0057-y>.
- Bliednick, D.M., Robertson, A.H.F., Sheridan, R.E., 1983. Deposition and provenance of Miocene intrastratal chalks, Blake-Bahama Basin, western North Atlantic. Initial reports of the Deep Sea Drilling Project. 44. U.S. Government Printing Office, Washington, D.C., pp. 727–748.
- Carlo, D.-L., 1996. Characterization of Rock-magnetic Signature During Subaerial Exposure in Platform Carbonates From New Providence, Bahamas. PhD Thesis Ohio state University 66 p.
- Cavailhes, T., Sizun, J.P., Labaume, P., Chauvet, A., Buatier, B., Soliva, R., Mezri, L., Charpentier, D., Leclère, H., Travé, A., Gout, C., 2013. Influence of fault rock foliation on fault zone permeability: The case of deeply buried arkosic sandstones (Grès d'Annot, southeastern France). *AAPG Bulletin* 97, 1521–1543. <https://doi.org/10.1306/03071312127>.
- Chanton, J.P., Martens, C.S., Paull, C.K., 1991. Control of pore-water chemistry at the base of the Florida escarpment by processes within the platform. *Nature* 349, 229–231.
- Chapron, E., Van Rensbergen, P., De Batist, M., Beck, C., Henriot, J.P., 2004. Fluid-escape features as a precursor of a large sublacustrine sediment slide in Lake Le Bourget, NW Alps, France. *Terra Nova* 16, 305–311. <https://doi.org/10.1111/j.1365-3121.2004.00566.x>.
- Cole, D., Stewart, S.A., Cartwright, J.A., 2000. Giant irregular pockmark craters in the Palaeogene of the Outer Moray Firth Basin, UK North Sea. *Mar. Pet. Geol.* 17, 563–577.
- Corbella, M., Ayora, C., Cardellach, E., 2004. Hydrothermal mixing, carbonate dissolution and sulfide precipitation in Mississippi valley-type deposits. *Mineral. Deposita* 39, 344–357. <https://doi.org/10.1007/s00126-004-0412-5>.
- Cornet, T., Cordier, D., Le Bahers, T., Bourgeois, O., Fleurant, C., Le Mouélic, S., Altobelli, N., 2015. Dissolution on Titan and on Earth: toward the age of Titan's karstic landscapes. *J. Geophys. Res. Planets* 120, 1044–1074. <https://doi.org/10.1002/2014JE004738>.
- D'Angeli, I.M., Parise, M., Vattano, M., Madonia, G., Galdenzi, S., De Waele, J., 2019. Sulfuric acid caves of Italy: a review. *Geomorphology* 333, 105–122.
- Dando, P.R., Austen, M.C., Burke Jr., R.A., Kendall, M.A., Kennicutt II, M.C., Judd, A.G., Moore, D.C., O'Hara, S.C.M., Schmaljohann, R., Southward, A.J., 1991. Ecology of a North Sea pockmark with an active methane seep. *Mar. Ecol. Prog. Ser.* 70, 49–63.
- Dawans, J.M., Swart, P.K., 1988. Textural and geochemical alternations in late Cenozoic Bahamian dolomites. *Sedimentology* 35, 385–403. <https://doi.org/10.1111/j.1365-3091.1988.tb00993.x>.
- Dickens, G.R., 2003. Rethinking the global carbon cycle with a large, dynamic and microbially mediated gas hydrate capacitor. *Planet. Sci. Lett.* 213, 169–183.
- Etiopie, G., Papatheodorou, G., Christodoulou, P., Ferentinos, G., Sokos, E., Favali, P., 2006. Methane and hydrogen sulfide seepage in the Northwest Peloponnesus petroliferous basin (Greece): origin and geohazard. *AAPG Bull.* 90 (5), 701–713. <https://doi.org/10.1306/11170505089>.
- Foland, S., Maher, N., Yun, J., 1999. Pockmarks along the California continental margin; implications for fluid-flow. *AAPG Bull.* 83, 687–688.
- Ford, D.C., Williams, P., 2007. *Karst Hydrogeology and Geomorphology*. Wiley, Chichester, p. (562 pp.).
- Freeman-Lynde, R.P., Cita, M.B., Jadoul, F., Miller, E.L., Ryan, W.B.F., 1981. Marine geology of the Bahama Escarpment. *Mar. Geol.* 44, 119–156.
- Freeman-Lynde, R.P., Ryan, W.B.F., 1985. Erosional modification of Bahama Escarpment. *Geol. Soc. Am. Bull.* 96, 481–494.
- Garcia-Rios, M., Luquot, L., Soler, J.M., Cama, J., 2015. Influence of the flow rate on dissolution and precipitation features during percolation of CO₂-rich sulfate solutions through fractured limestone samples. *Chem. Geol.* 414, 95–108.
- Garven, H., Freeze, R.A., 1994. Theoretical analysis of the role of groundwater flow in the genesis of stratatound ore deposits: quantitative results. *American Journal of science* 284 (10), 1125–1174. <https://doi.org/10.2475/ajs.284.10.1125>.
- Gay, A., Lopez, M., Cochon, P., Sultan, N., Cauquil, E., Brigaud, F., 2003. Sinuous pockmark belt as indicator of a shallow buried turbiditic channel on the lower slope of the Congo Basin, West African Margin. In: Van Rensbergen, P., Hillis, R.R., Maltman, A.J., Morley, C.K. (Eds.), *Subsurface Sediment Mobilization*. Special Publications. Geological Society of London, London, pp. 173–189.
- Gay, A., Lopez, M., Potdevin, J.-L., Vidal, V., Varas, G., Favier, A., Tribouillard, N., 2019. 3D morphology and timing of the giant fossil pockmark of Beauvoisin, SE Basin of Franc. *J. Geol. Soc.* 176, 61–77. <https://doi.org/10.1144/jgs2018-064>.
- Gutiérrez, F., Guerrero, J., Lucha, P., 2008. A genetic classification of sinkholes illustrated from evaporite paleokarst exposures in Spain. *Environ. Geol.* 53 (5), 993–1006.
- Gutiérrez, F., Parise, M., De Waele, J., Jourde, H., 2014. A review on natural and human-induced geohazards and impacts in Karst. *Earth Sci. Rev.* 138, 61–88. <https://doi.org/10.1016/j.earscirev.2014.08.002>.
- Gouze, P., Noiriél, C., Bruderer, C., Loggia, D., Leprovost, R., 2003. X-ray tomography characterization of fracture surfaces during dissolution. *Geophysical Research Letter* 30 (5), 1267. <https://doi.org/10.1029/2002GL016755>.
- Heath, K.C., Mullins, H.T., 1984. Open-ocean, off-bank transport of fine-grained carbonate sediments in the northern Bahamas. In: Stow, D.A.V., Piper, D.J.W. (Eds.), *Fine-grained Sediments: Deep-water Processes and Facies*. 15. Spec. Publ. Geol. Soc. Lond. Blackwell Scientific Publications, Oxford, pp. 199–208. <https://doi.org/10.1144/GSL.SP.1984.015.01.13>.
- Henderson, G.M., Slowey, N.C., Haddad, G.A., 1999. Fluid flow through carbonate platforms: constraints from 234U/238U and Cl- in Bahamas pore-waters. *Earth and Planetary Science Letters* 169, 99–111.
- Hill, C.A., 1990. Sulfuric acid speleogenesis of Carlsbad Cavern and its relationship to hydrocarbons, Delaware Basin, New Mexico and Texas. *AAPG Bulletin* 74 (11), 1685–1694.
- Hiller, T., Romanov, D., Gabrovsek, F., Kaufmann, G., 2014. The creation of collapse dolines: a 3D modeling approach. *Acta Carsologica* 43 (2–3).
- Hollister, C.D., Ewing, J.I., Habib, D., Hathaway, J.C., Lancelot, Y., Luterbacher, H., Paulus, F.J., Poag, C.W., Wilcox, J.A., Worstell, P., 1972. Deep Sea Drilling Program Volume XI, Shipboard Site Reports, Site 99. 1972. Cat Gap. <https://doi.org/10.2973/dsdp.proc.11.102>.
- Hollister, C.D., Ewing, J.I., Habib, D., Hathaway, J.C., Lancelot, Y., Luterbacher, H., Paulus, F.J., Poag, C.W., Wilcox, J.A., Worstell, P., 1972b. Deep Sea Drilling Program volume XI, Shipboard Site Reports, Site 100. Cat Gap <https://doi.org/10.2973/dsdp.proc.11.103.1972>.
- Hornbach, M.J., Ruppel, C., Van Dover, C.L., 2007. Three-dimensional structure of fluid conduits sustaining an active deep marine cold seep. *Geophys. Res. Lett.* 34 (5), L05601. <https://doi.org/10.1029/2006GL028859>.
- Hovland, M., Gardner, J.V., Judd, A.G., 2002. The significance of pockmarks to understanding fluid flow processes and geohazards. *Geofluids* 2, 127–136.
- Hughes, J.D., Vacher, H.L., Sanford, W.E., 2007. Three-dimensional flow in the Florida platform: theoretical analysis of Kohout convection at its type locality. *Geology* 35 (7), 663–666. <https://doi.org/10.1130/G23374A.1>.
- Judd, A.G., Hovland, M., 2009. *Seabed Fluid Flow: The Impact of Geology, Biology and the Marine Environment*. Cambridge Univ. Press.
- Kaufmann, G., Braun, J., 1999. Karst aquifer evolution in fractured rocks. *Water Resour. Res.* 35 (11), 3223–3238.
- Kindler, P., Godefroid, F., Chiaradia, M., Ehlert, C., Eisenhauer, A., Frank, M., Hasler, C.-A., Samankassou, E., 2011. Discovery of Miocene to early Pleistocene deposits on Mayaguana, Bahamas: evidence for recent active tectonism on the north american margin. *Geology* 39, 523–526.
- King, L.H., MacLean, B., 1970. Pockmarks on the Scotian Shelf. *Bull. Geol. Soc. Am.* 81, 3141–3148.
- Klimchouk, A., 2009. Morphogenesis of hypogenic caves. *Geomorphology* 106, 100–117. <https://doi.org/10.1016/j.geomorph.2008.09.013>.
- Kohout, F.A., Henry, H.R., Banks, J.E., 1977. Hydrogeology related to the geothermal conditions of the Florida Plateau. Florida Bureau of Geology Special Publication 21, 1–39.
- Komatsu, G., Ori, G.G., Cardinale, M., Dohm, M.J., Baker, V.R., Vaz, D.A., Ishimaru, R., Namiki, N., Matsui, T., 2011. Roles of methane and carbon dioxide in geological processes on Mars. *Planet. Space Sci.* 59, 169–181.
- La Bruña, V., Bezerra, F.H.R., Souza, V.H.P., Maiá, R.P., Auler, A.S., Araujo, R.E.B., Cazarin, C.L., Rodrigues, M.A.F., Vieira, L.C., Sousa, M.O.L., 2021. High permeability zones in folded and faulted silicified carbonate rocks: implications for karstified carbonate reservoir. *Mar. Pet. Geol.* 105046. <https://doi.org/10.1016/j.marpetgeo.2021.105046>.
- Land, L.A., Paull, C.K., Hobson, B., 1995. Genesis of a submarine sinkhole without subaerial exposure: Straits of Florida. *Geology* 23 (10), 949–951.
- Land, L.A., Paull, C.K., Spiess, F.N., 1999. Abyssal erosion and scarp retreat: Deep Tow observations of the Blake Escarpment and Blake Spur. *Mar. Geol.* 160, 63–83.
- Land, L.A., Paull, C.K., 2000. Submarine karst belt rimming the continental slope in the Straits of Florida. *Geo-Mar. Lett.* 20, 123–132.
- Lee, T.N., Johns, W.E., Zantopp, R.J., Fillenbaum, E.R., 1996. Moored observations of Western Boundary current variability and thermohaline circulation at 26.5°N in the subtropical North Atlantic. *J. Phys. Oceanogr.* 26, 962–983.
- Lu, X., Wang, Y., Tian, F., Li, X., Yang, D., Li, Tao, Lv, Y., He, X., 2017. New insights into the carbonate karstic fault system and reservoir formation in the Southern Tahe area of the Tarim Basin. *Marine and Petroleum Geology*, 86, pp. 587–605. <https://doi.org/10.1016/j.marpetgeo.2017.06.023>.
- Makovsky, Y., Klemperer, S.L., 1999. Measuring the seismic properties of Tibetan bright spots: Evidence for free aqueous fluids in the Tibetan middle crust. *J. Geophys. Res.* 104, 10795–10825.
- Marcon, Y., Ondréas, H., Sahling, H., Bohrmann, G., Olu, K., 2014. Fluid-flow regimes and growth of a giant pockmark. *Geology* 42 (1), 63–66. <https://doi.org/10.1130/G34801.1>.
- Masafferro, J.L., Bulnes, M., Poblet, J., Eberli, G.P., 2002. Episodic folding inferred from syntectonic carbonate sedimentation: the Santaren anticline, Bahamas foreland. *Sedimentary Geology* (ISSN: 0037-0738) 146 (1–2), 11–24. [https://doi.org/10.1016/S0037-0738\(01\)00163-4](https://doi.org/10.1016/S0037-0738(01)00163-4).
- Melim, L., Masafferro, J.-L., 1997. Subsurface geology of the Bahamas banks. In: Vacher, H.L., Quinn, T.M. (Eds.), *Geology and Hydrogeology of Carbonate Islands*. Elsevier Science B.V., Amsterdam, Netherlands, pp. 161–182.

- Mercier de Lépinay, M., Loncke, L., Basile, C., Roest, W.R., Patriat, M., Maillard, A., De Clarens, P., 2016. Transform continental margins – part 2: a worldwide review. *Tectonics* 693, 96–115.
- Micallef, A., Berndt, C., Debono, G., 2011. Fluid flow systems of the Malta Plateau, Central Mediterranean Sea. *Mar. Geol.* 284 (1–4), 74–85.
- Michaud, F., Chabert, A., Collot, J.-Y., Sallarès, V., Flueh, E.R., Charvis, P., Graindorge, D., Guster, M.-A., Billas, J., 2005. Fields of multi-kilometer scale sub-circular depressions in the Carnegie Ridge sedimentary blanket: effect of underwater carbonate dissolution. *Mar. Geol.* 216, 205–219.
- Michaud, F., Collot, J.Y., Ratzov, G., Proust, J.N., Dano, A., Lebrun, J.F., Hernandez, M.J., Loayza, G., Khaoulani, A., Stoll, Y., Poudroux, H., De Min, L., 2018. A honeycomb seafloor morphology in carbonate sediment of the Carnegie Ridge (offshore Ecuador): formation and potential geodynamic significance. *Geology* 46, 979–982. <https://doi.org/10.1130/G45285.1>.
- Mitchell-Tapping, H., Bellucci, R.B., Woody, G., Lee, T.J., 1999. Mud hole: a unique warm-water submarine spring, located offshore southwestern Florida: Gulf Coast Association of geological societies. *Transactions* 49, 370–383.
- Mulder, T., Gillet, H., Hanquiez, V., Reijmer, J.J.G., Droxler, A.W., Recouvreur, A., Fabregas, N., Cavailles, T., Fauquembergue, K., Blank, D.G., Guaiastrennec-Faugas, L., Seibert, C., Bashah, S., Bujan, S., Ducassou, E., Principaud, M., Conesa, G., Le Goff, J., Ragusa, J., Busson, J., Borgomano, J., 2019. Into the deep: A coarse-grained carbonate turbidite valley and canyon in ultra-deep carbonate setting. *Marine Geology* 407, 316–333. <https://doi.org/10.1016/j.margeo.2018.11.003>.
- Mulder, T., 2016. CARAMBAR 2 cruise. RV l'Atalante <https://doi.org/10.17600/16001500>.
- Mulder, T., Gillet, H., Hanquiez, V., Ducassou, E., Fauquembergue, K., Principaud, M., Conesa, G., Le Goff, J., Ragusa, J., Bashah, S., Bujan, S., Reijmer, J.J.G., Cavailles, T., Droxler, A.W., Blank, D.G., Guaiastrennec-Faugas, L., Fabregas, N., Recouvreur, A., Seibert, C., 2018. Carbonate slope morphology revealing a giant submarine canyon (Little Bahama Bank, Bahamas). *Geology* 46, 31–34. <https://doi.org/10.1130/G39527.1>.
- Mullins, H.T., Lynts, G.W., 1977. Origin of the northwestern Bahama Platform: Review and Reinterpretation. *GSA Bulletin* 88, 1447–1461. [https://doi.org/10.1130/0016-7606\(1977\)88<1447:OOTNBP>2.0.CO;2](https://doi.org/10.1130/0016-7606(1977)88<1447:OOTNBP>2.0.CO;2).
- Mullins, H.T., Mark Van Buren, H., 1981. Walkers Cay Fault, Bahamas: evidence for Cenozoic faulting. *Geo-Mar. Lett.* 1, 225–231. <https://doi.org/10.1007/BF02462438>.
- Mullins, H., Breen, N., Dolan, J., Wellner, W., Petruccione, J.L., Gaylord, M., Andersen, B., Melillo, A.J., Jurgens, A.D., Orange, D., 1992. Carbonate platforms along the Southeast Bahamas-Hispaniola collision zone. *Mar. Geol.* 105, 169–209.
- Ondréas, H., Fouquet, K.O., Charlou, J.L., Gay, A., Dennielou, B., Donval, J.P., Fifs, A., Nadalig, T., Cochonat, P., Cauquil, E., Bourillet, J.F., Le Moigne, M., Sibuet, M., 2005. ROV study of a giant pockmark on the Gabon continental margin. *Geo-Mar. Lett.* 25 (5), 281–292.
- Orange, D.L., Yun, J., Maher, N., Barry, J., Greene, G., 2002. Tracking California seafloor seeps with bathymetry, backscatter and ROVs. *Cont. Shelf Res.* 22 (16), 2273–2290.
- Parise, M., 2019. Sinkholes. In: Culver, D.C., White, W.B., Pipan, T. (Eds.), *Encyclopedia of Caves*. Academic Press, pp. 934–942.
- Paull, C.K., Dillon, W.P., 1980. Erosional origin of the Blake Escarpment: an alternative hypothesis. *Geology* 8, 538–542.
- Paull, C., Neumann, A.C., 1987. Continental margin brine seeps: their geological consequences. *Geology* 15, 545–548.
- Paull, C.K., Spiess, F.N., Curray, J.R., Twitchell, D., 1988. Morphology of Florida Escarpment chemosynthetic brine seep community sites: deep-tow, seabeam, and GLORIA surveys. Conference: Annual Meeting of the American Association of Petroleum Geologists, Houston, TX, USA, 20–23 March. 72, p. 2.
- Paull, C.K., Commeau, R.F., Curry, J.R., Neumann, A.C., 1991. Seabed measurements of modern corrosion rates on the Florida escarpment. *Geo-Mar. Lett.* 1, 16–22.
- Pilcher, R., Argent, J., 2007. Mega-pockmarks and linear pockmark trains on the West African continental margin. *Mar. Geol.* 244, 15–32. <https://doi.org/10.1016/j.margeo.2007.05.002>.
- Pisani, L., Antonellini, M., D'Angeli, I.M., De Waele, J., 2021. Structurally controlled development of a sulfuric hypogene karst system in a fold-and-thrust belt (Majella Massif, Italy). *J. Struct. Geol.* 145, 104305.
- Pontes, C.C., Bezerra, F.H., Bertotti, G., La Bruna, V., Audra, P., De Waele, J., Pisani, L., 2021. Flow pathways in multiple direction fold hinges: implications for fractured and karstified carbonate reservoirs. *J. Struct. Geol.* 146, 104324.
- Privalov, V., Randi, A., Sterpenich, J., Pironon, J., Morlot, C., 2019. Structural control of a dissolution network in a limestone reservoir forced by radial injection of CO₂ saturated solution: Experimental results coupled with X-Ray computed tomography. *Geosciences* 9 (1), 33.
- Post, V.E.A., Groen, J., Kooi, H., Person, M., Ge, S., Edmunds, W.M., 2013. Offshore fresh groundwater reserves as a global phenomenon. *Nature* 504, 71–78. <https://doi.org/10.1038/nature12858>.
- Rosenberg, J.H., 2019. Erosion of the Florida and Yucatan carbonate margins of the gulf of Mexico: subaqueous or subaerial? *Geogulf Transactions*. 69, pp. 263–278
- Rotevatn, A., Bastesen, E., 2014. Fault linkage and damage zone architecture in tight carbonate rocks in the Suez Rift (Egypt): implications for permeability structure along segmented normal faults. In: Spence, G.H., et al. (Eds.), *Advances in the Study of Fractured Reservoirs*. 374. Geological Society of London Special Publication, pp. 79–95. <https://doi.org/10.1144/SP374.1>.
- Salmi, M.S., Johnson, H.P., Leifer, I., Keister, J.E., 2011. Behavior of methane seep bubbles over a pockmark on the Cascadia continental margin. *Geosphere* 7 (6), 1273–1283. <https://doi.org/10.1130/GES00648.1>.
- Sanford, W., Konikow, L., 1989. Porosity development in coastal carbonate aquifers. *Geology* 17, 249–252.
- Sauro, U., 2003. Dolines and sinkholes: aspects of evolution and problems of classification. *Acta Carsol* 32 (2), 41–52.
- Sauro, F., Mecchia, M., Piccini, L., De Waele, J., Carbone, C., Columbu, A., Vergara, F., 2019. Genesis of giant sinkholes and caves in the quartz sandstone of Sarisariñama tepui, Venezuela. *Geomorphology* 342, 223–238.
- Schlager, W., Corso, W., McNulty, C.L., Fluegel, E., Renz, O., Steinmetz, J.C., Austin Jr., J.A., 1984. Early Cretaceous platform re-entrant and escarpment erosion in the Bahamas. *Geology* 12, 147–150.
- Shaw, J., Courtney, R.C., Currie, J.R., 1997. Marine Geology of Saint George's Bay, Newfoundland, as interpreted from multibeam bathymetry and back-scatter data. *Geo-Mar. Lett.* 17, 188–194.
- Sheridan, R.E., 1974. Conceptual Model for the Block-fault origin of the north American Atlantic Continental margin Geosyncline. *Geology* 2 (9), 465–468. [https://doi.org/10.1130/0091-7613\(1974\)2<465:CMFTBO>2.0.CO;2](https://doi.org/10.1130/0091-7613(1974)2<465:CMFTBO>2.0.CO;2).
- Sibson, R., 1996. Structural permeability of fluid-driven fault-fracture meshes. *Journal of structural Geology* 18 (8), 1031–1042. [https://doi.org/10.1016/0191-8141\(96\)00032-6](https://doi.org/10.1016/0191-8141(96)00032-6).
- Simms, M., 1984. Dolomitization by thermal convection in carbonate platforms: Abstract. *AAPG Bull.* 68 (4), 528.
- Staudigel, P., Higgins, J., Swart, P.K., 2021. An abrupt Middle-Miocene increase in fluid-flow into the Leeward margin Great Bahama Bank, constraints from $\delta^{44}\text{Ca}$ and $\Delta 47$ values. *Earth Planet. Sci.* 553, 116625. <https://doi.org/10.1016/j.epsl.2020.116625>.
- Sultan, N., Marsset, B., Ker, S., Marsset, T., Voisset, M., Vernant, A.M., Bayon, G., Cauquil, E., Adamy, J., Colliat, J.L., Drapeau, D., 2010. Hydrate dissolution as a potential mechanism for pockmark formation in the Niger Delta. *J. Geophys. Res.* 115, B08101. <https://doi.org/10.1029/2010JB007453>.
- Taylor, M.H., Dillon, W.P., Pecher, I.A., 2000. Trapping and migration of methane associated with the gas hydrate stability zone at the Blake Ridge Diapir: new insights from seismic data. *Mar. Geol.* 164, 79–89.
- Warren, J.K., 2016. Salt dissolution and pointers to vanished evaporites: Karst, breccia, nodules and cement. *Evaporites*. Springer, Cham https://doi.org/10.1007/978-3-319-13512-0_7.
- Walles, F.E., 1993. Tectonic and diagenetically induced seal failure within the southwestern Great Bahamas Bank. *Mar. Pet. Geol.* 10, 14–28.
- Webb, K.E., 2009. Ecology and Geology of Pockmarks. Physics of Geological Processes Department of Biology, Faculty of Mathematics and Natural Sciences University of Oslo, p. 49.
- Whitaker, F.F., Smart, P.L., 1990. Active circulation of saline ground waters in carbonate platforms: evidence from the Great Bahama Bank. *Geology* 18, 200–203.
- Whitaker, F.F., Smart, P.L., 1993. Circulation of saline groundwaters in carbonate platforms: A review and case study from the Bahamas. In: Horbury, A.D., Robinson, A.G. (Eds.), *Diagenesis and Basin Development*. Am. Assoc. Petrol. Geol. Studies Geol36, pp. 113–132.
- Whitaker, F.F., Smart, P.L., Vahrenkamp, V.C., Nicholson, H., Wogelius, R.A., 1994. Dolomitization by near-normal seawater? Field evidence from the Bahamas. In: Purser, B.H., Tucker, M., Zenger, D.H. (Eds.), *Dolomites, A volume in Honour of Dolomieu*. 21. International Association of Sedimentology Special Publication, pp. 111–132.
- Wierzbicki, R., Dravis, J., Al-Aasnm, Harland, N., 2006. Burial dolomitization and dissolution of Upper Jurassic Abenaki platform carbonates, Deep Panuke reservoir, Nova Scotia, Canada. *The American Association of Petroleum Geologists* 90 (11), 1843–1861. <https://doi.org/10.1306/03200605074>.
- Wilson, A.M., 2005. Fresh and saline groundwater discharge to the ocean: a regional perspective. *Water Resources Research* 41, W02016. <https://doi.org/10.1029/2004WR003399>.
- Yeichieli, Y., Abelson, M., Baer, G., 2015. Sinkhole formation and subsidence along the Dead Sea coast, Israel. *Hydrogeol. J.* <https://doi.org/10.1007/s10040-015-1338-y>.
- Yubko, V.M., Lygina, T.I., 2015. Intraplate volcanic-hydrothermal systems of the Clarion-Clipperton zone, Pacific Ocean. *Dokl. Earth Sci.* 462, 555–558.